ELSEVIER

Journal of Marine Systems 32 (2002) 153–179

JOURNAL OF MARINE SYSTEMS

www.elsevier.com/locate/jmarsys

A model for ocean circulation on the Iberian coast

H.S. Coelho [a,*], R.J.J. Neves [b], M. White [c], P.C. Leitão [b], A.J. Santos [b]

[a] *University of Algarve, Campus de Gambelas, 8000 Faro, Portugal*
[b] *Department of Mechanical Engineering, Instituto Superior Técnico, Av. Rovisco Pais, 1096 Lisbon, Portugal*
[c] *Department of Oceanography, NUI, Galway, Ireland*

Received 31 October 2000; accepted 27 June 2001

Abstract

We used a three-dimensional model with generic vertical coordinate to investigate the structure of flow and transports on the Iberian shelf-slope region. Two different types of experiments were conducted. The first was a process-oriented study to investigate the role of thermohaline forcing in the generation and meridional variability of the poleward slope current. The second experiment was a more realistic simulation for the year of 1994, a period for which there are several long-term current meter data sets available. Comparisons between model, data and other published works have shown a reasonable agreement both qualitatively and quantitatively. The results obtained included the seasonal cycle with upwelling during the summer and a winter surface poleward current over the shelf, with a permanent undercurrent transporting Mediterranean Water along the Portuguese and Spanish slopes. The along-slope transports were predominant especially in the OMEX II–II study area. The meridional transport is poleward all year round, decreasing from winter to summer and from the south to the north.

Keywords: Modelling; Iberia; Circulation; Fluxes; Exchange

1. Introduction

The eastern boundary current system off Iberia marks the northern limit of the Canary Current coastal upwelling system. The Canary Current forms the eastern limb of the subtropical gyre of the North Atlantic. West of Iberia, the flow is weak and towards the eastern boundary (Saunders, 1982; Paillet and Mercier, 1997). In summertime, coastal upwelling occurs in response to the trade winds, with associated equatorward flow that dominates the continental shelf and slope. Little is known about wintertime circulation other than the findings of a few papers published in the last 10 years (e.g. Haynes and Barton, 1990; Frouin et al., 1990). These studies indicate the presence of a surface poleward flow, which is relatively narrow and weak (Haynes and Barton, 1990; Frouin et al., 1990; Mazé et al., 1997). A poleward subsurface flow is very common in upwelling regions. The undercurrent generally has a width of less than 100 km and vertical extent of several hundred meters. Off Iberia, readings from several arrays of current meters have indicated that most of the water column flows poleward. It is well established that Mediterranean Water (MW) flows to the north along the continental slope as part of the undercurrent that probably extends from 1500 m to the bottom of the surface mixed layer (Ambar et al., 1986). During the winter, the poleward undercurrent shallows to the north and occasionally

* Corresponding author. Tel.: +351-89-800900x7166.
E-mail address: hcoelho.maretec@taguspark.pt (H.S. Coelho).

0924-7963/02/$ - see front matter
PII: S0924-7963(02)00032-5

reaches the surface. Although the current is described as existing to the north of Cabo da Roca (see Fig. 1), recent observations show that there is also a surface poleward current on the southern coast that sometimes reaches Cabo São Vicente, turning to the north along the southwest coast of Portugal (Relvas, 1999).

The mechanism behind the seasonality of the flow along western Iberia is probably the seasonal migration of the semi-permanent subtropical high-pressure system known as the Azores High. The center of the Azores High migrates meridionally between 27°N in March and 33°N in August. Consequently, the pressure difference between the center of the Azores High and Portugal varies from 1 mbar in the winter to 8 mbar in the summer, leading to stronger north/northwesterly winds in summertime, which are favourable

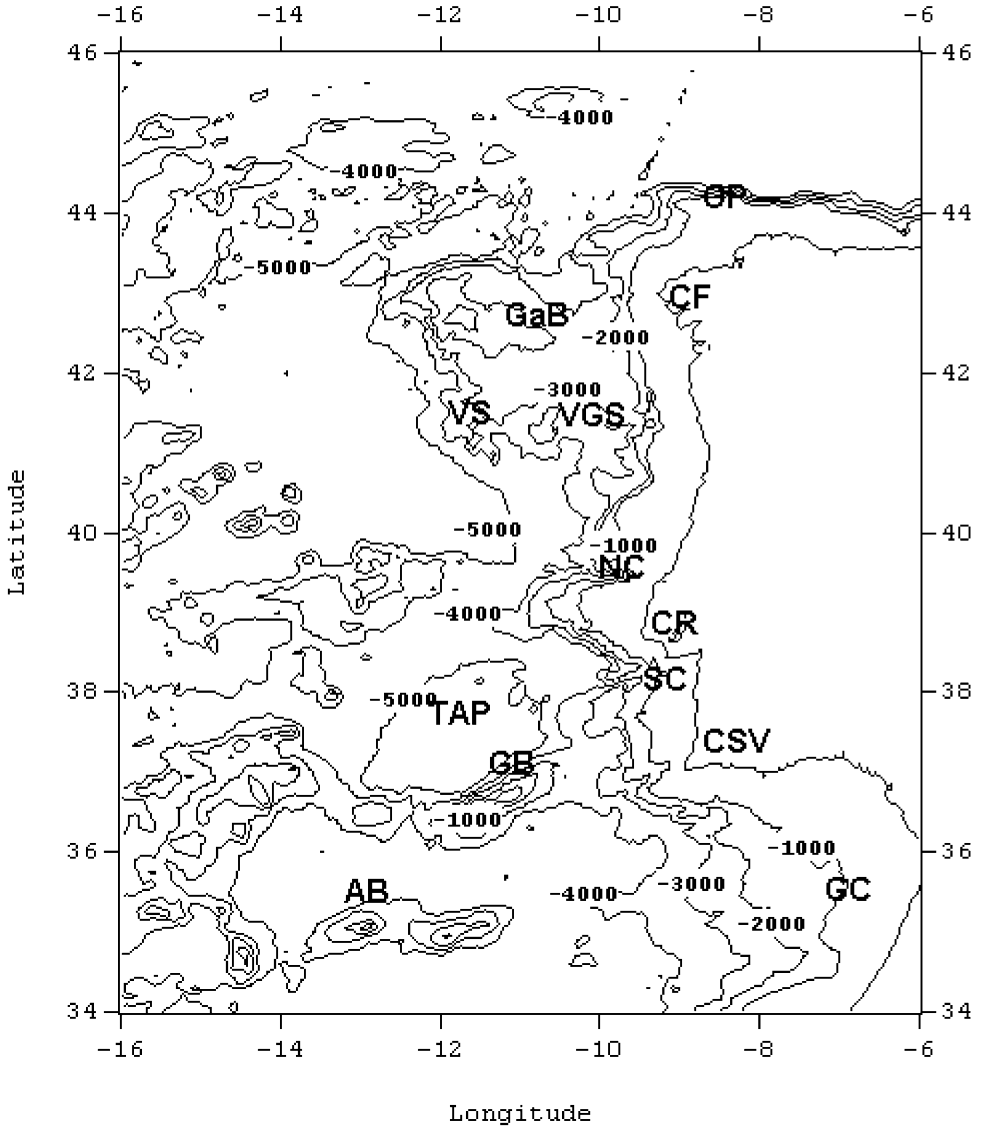

Fig. 1. Model domain with reference to prominent features. GC — Gulf of Cadiz; AB — Ampére Bank; GB — Gorringe Bank; TAP — Tagus Abyssal Plain; CSV — Cape S. Vicente; SC — Setúbal Canyon; CR — Cape Roca; NC — Nazaré Canyon; VGS — Vasco da Gama Seamount; VS — Vigo Seamount; GaB — Galicia Bank; CF — Cape Finisterre; OP — Ortegal Promontory.

to upwelling, together with the generation of associated upwelling filaments — cool bands of water extending out from the shelf into the deep ocean (Haynes et al., 1993). During the winter, this northerly component of the wind weakens, or even reverses, leading to a reversal of the surface flow that can be identified in satellite images as a warm poleward current (Haynes and Barton, 1990).

Over the last 20 years, several modelling studies of eastern boundary current systems have been published, particularly for the California Current system and for the Leeuwin Current. McCreary et al. (1987) conducted experiments using a linear model with both transient and steady wind forcing in the California Current system. The results were very weak currents (<10 cm/s) with no eddies, meanders or filaments. The studies published by Weaver and Middleton (1990), Batteen and Rutherford (1990) and Batteen et al. (1992) focus on the modelling of wind and thermohaline forcing off western Australia. In the latest of these studies, the authors were able to reproduce most of the mesoscale variability observed. In contrast to the two regions described above, only a handful of modelling studies of the Iberian and Northwest African coasts have been carried out. More recently, Batteen et al. (2000) published a study of wind and thermohaline forcing in an area containing part of Iberia and the northwest of Africa. Their findings highlight the major characteristics and unique features of the northern Canary Current system. Other studies include those by Jungclaus and Mellor (2000) on the Mediterranean Outflow and Meddy formation, and by Stevens et al. (2000) and Røed and Shi (1999), both within the framework of the EU MORENA project, on circulation off western Iberia and the dynamics of cool filaments, respectively. The study by Stevens et al. (2000) has produced findings in closer agreement with data obtained in several cruises made as part of the MORENA project.

The modelling work presented here has been carried out within the framework of the Ocean Margin EXchange project (OMEX) and aims to contribute to a better understanding of circulation off western Iberia. Since the area of interest for OMEX was the Galician shelf/slope region, our main objective was to estimate volume transports in the area and to carry out model validation experiments. This can be a difficult task, as data is not generally collected solely for the purpose of comparison with models. During OMEX II–II, over 40 current meter years of historical pre-OMEX data in the region of northwest Iberia were analysed and statistics compiled (Huthnance et al., 2002). Our approach was: (1) to compare current statistics obtained with the model and with measured data, (2) to identify circulation patterns identified from the data and compare them with model results and (3) to use measured transports estimated from the data to validate the model. In Section 2, we briefly describe the model used for the simulations. In Section 3, we describe the results obtained in two different types of numerical experiments: (1) using only thermohaline forcing and (2) using thermohaline and realistic wind forcing. We analyse the model results in detail and then use current meter data to show that the magnitudes of velocities and transports are correct. Finally, we attempt to estimate the exchanges between the shelf/slope area and the deep ocean off Galicia in an area enclosed between 42°N and 43°N and delimited to the west at 10.5°W (further details on box definition can be found in Huthnance et al., 2002).

2. The model

2.1. Equations

Modelling the interaction of a slope system and a stratified fluid is a difficult undertaking. It requires a fine resolution that in turn implies a limited extent model, and therefore the knowledge of boundary conditions that are not easy to assess. There have, however, been some successful studies of this kind. Examples include the simulation of the Norwegian coastal current by Oey and Chen (1992), the simulation of the California Current System by Marschesiello et al. (2001), and the simulation of the Iberian coastal current system by Stevens et al. (2000).

The model used in this work is MOHID2000, which was originally developed by Santos (1995) at the Instituto Superior Técnico (IST) in Lisbon. Early versions of MOHID2000 used sigma coordinates in the vertical. More recently, MOHID2000 has evolved to a generic vertical coordinate model (Martins et al., 1998; Martins et al., 2001). The model has been used in several estuarine and oceanic applications (Cancino and Neves, 1998; Taboada et al., 1998; Martins

et al., 1999; Coelho et al., 1999; Miranda et al., 1999). A detailed description of the model can be found in Martins et al. (2001). MOHID2000 solves the three-dimensional primitive equations in Cartesian coordinates for incompressible flows. Hydrostatic equilibrium is assumed, as is as Boussinesq approximation. Mass and momentum evolution equations are:

$$\frac{\partial u_i}{\partial x_i} = 0 \tag{1}$$

$$\frac{\partial u_1}{\partial t} + \frac{\partial (u_j u_1)}{\partial x_j} = -fu_2 - g\frac{\rho_\eta}{\rho_0}\frac{\partial \eta}{\partial x_1} - \frac{1}{\rho_0}\frac{\partial p_s}{\partial x_1} - \frac{g}{\rho_0}\int_z^\eta \frac{\partial \rho'}{\partial x_1}\mathrm{d}x_3 + \frac{\partial}{\partial x_j}\times\left(A_j\frac{\partial u_1}{\partial x_j}\right) \tag{2}$$

$$\frac{\partial u_2}{\partial t} + \frac{\partial (u_j u_2)}{\partial x_j} = fu_1 - g\frac{\rho_\eta}{\rho_0}\frac{\partial \eta}{\partial x_2} - \frac{1}{\rho_0}\frac{\partial p_s}{\partial x_2} - \frac{g}{\rho_0}\int_z^\eta \frac{\partial \rho'}{\partial x_2}\mathrm{d}x_3 + \frac{\partial}{\partial x_j}\times\left(A_j\frac{\partial u_2}{\partial x_j}\right) \tag{3}$$

$$\frac{\partial p}{\partial x_3} = -\rho g \tag{4}$$

where u_i are the velocity vector components in Cartesian x_i directions positive to the east, to north and upward, η is the free surface elevation, f is the Coriolis parameter, A_i the turbulent viscosity and p_s is the atmospheric pressure. ρ is the density and ρ' its anomaly. Density is calculated as a function of temperature and salinity by the equation of state (Leendertsee and Liu, 1978):

$$\rho = (5890 + 38T - 0.375T^2 + 3S)/((1779.5 + 11.25T - 0.0745T^2) - (3.8 + 0.01T)S + 0.698(5890 + 38T - 0.375T^2 + 3S)) \tag{5}$$

The computed flow field transports salinity, temperature and other tracers using an advection–diffusion equation.

The model uses a semi-implicit ADI algorithm with two time levels per iteration. Two numerical schemes are currently implemented: the four-equation S21 scheme (Abbot et al., 1973), and the six-equation Leendertsee scheme (Leendertse, 1967).

The model solves the equations in the real domain without any space transformation. The geometry information is stored in the areas and volumes needed to calculate fluxes. Therefore, a complete separation between the hydrodynamic variables and the geometry is accomplished for all grid types. The geometry information is updated every time step by a function that expresses the dependency on the grid type. The computational effort necessary to perform this calculation is comparable to that used in solving the Jacobean of the transformation, while the method is much more flexible (Vinokur, 1989). Cells are permitted any initial shape and can undergo any time deformation. This flexible architecture is compatible with a generic vertical coordinate. The same code can be used with several vertical-layering schemes. In this model, the domain can be divided vertically into subdomains and a different grid law can be applied to each subdomain. The computational cells have some restrictions on their geometry in order to reduce the storage and computational requirements of the model. The vertices have only 1 degree of freedom, along the vertical; the horizontal plane is fixed. The U_i velocity cells are staggered in an Arakawa C-grid (Arakawa and Lamb, 1977).

Free surface elevation is computed through integration of Eq. (1) over the water column. The two components of the horizontal velocity are globally centred in $t + 1/2$ leading to a second-order time accuracy (Martins et al., 2001). Vertical fluxes are also computed by continuity (considering the hydrostatic approach), integrating over each cell volume. Since the grid is allowed to move on the vertical axis, the computation of the vertical fluxes and the redefinition of the geometry are calculated together.

For horizontal diffusion of heat, salt and momentum, a choice can be made between Laplacian or biharmonic operators with constant coefficients. For this study, the biharmonic operator proved to be more appropriate for the spatial scales involved. Bottom

stress is parameterised using a quadratic law. Vertical eddy viscosity/diffusivity is determined using a turbulence closure model selected from those available in the General Ocean Turbulence Model (Burchard et al., 1999) incorporated in MOHID2000. In this study, a simplified version of the model proposed by Gaspar et al. (1990) was used since it gives reasonable results without excessively increasing use of CPU resources.

2.2. Experimental design and forcing

The model domain encompasses the west coasts of Iberia and Morocco, extending from 32°N to 46°N and from 6°W to 16°W. Horizontal grid spacing is 8.5 km in both directions. Bottom topography was derived from ETOPO5 by means of an interpolation for the model grid followed by smoothing with a five-point Laplacian filter. The bottom depth is then determined, using shaved cells (Visbeck et al., 1997). The model uses 18 vertical layers centered at constant z-levels at depths of 5, 20, 45, 80, 130, 200, 290, 400, 530, 680, 850, 1040, 1250, 1480, 1750, 2200, 3000 and 4250 m. The choice of a z-level configuration for vertical coordinates is based on several tests in which sigma and double sigma coordinates are also used. However, with these configurations, the model systematically overestimates the along-slope flow. This is partially related with the so-called pressure gradient error with sigma coordinates. A similar conclusion was presented by Barnard et al. (1997) with the models used in the DYNAMO project.

Biharmonic heat, salt and momentum diffusion coefficients are set to 2×10^9 m^4 s^{-1}, a value equal to the one used by Batteen et al. (2000) with a similar horizontal resolution.

2.2.1. Lateral boundary conditions

Normal and tangential velocities are set to zero at the sidewalls. Fresh water river input at coastal boundaries is not considered in this study. The western, southern and northern boundaries are open, while the eastern boundary is open only at the Strait of Gibraltar. At the open boundaries, we need some conditions for the prognostic variables: sea surface height, barotropic velocity, baroclinic velocity, temperature and salinity. The set of boundary conditions used is very similar to the FOA scheme conceived by Palma and Matano (2000). This scheme is basically the same as the one used by Oey and Chen (1992). It consists of imposing the barotropic transports at the open boundary that are consistent with the density field, and at the same time allowing waves that are generated inside the domain to radiate out.

2.2.2. Barotropic velocities and sea surface height

The barotropic velocities at the open boundary are deduced from steady seasonal transports (the method of implementation is discussed below). Additionally, for the normal component of barotropic velocity ($\overline{u_n}$) we use a radiation condition proposed by Flather (1976):

$$\overline{u_n} = \overline{u_n^{clim}} - \sqrt{\frac{g}{H}}(\eta - \eta^{clim}) \tag{6}$$

This condition allows volume conservation and is very simple to apply.

2.2.3. Baroclinic velocities

Sommerfeld's one-dimensional radiation condition is applied for the normal baroclinic velocities at the boundary:

$$\frac{\partial \phi}{\partial t} \pm c_i \frac{\partial \phi}{\partial x} = -\frac{\phi}{\tau} \tag{7}$$

where ϕ stands for u and v, c_i is the fixed baroclinic internal wave speed, τ is a relaxation time scale and the plus (minus) sign applies to the right (left) open boundary. Eq. (7) is solved using an implicit upstream method for the partial derivatives, and the internal wave speed is fixed at $\sqrt{gH \times 10^{-3}}$, where H is the local depth.

2.2.4. Scalars: temperature and salinity

Our boundary condition for scalars is exactly the same as the one proposed by Oey and Chen (1992):

$$\frac{\partial \phi}{\partial t} + u \frac{\partial \phi}{\partial x} = 0 \tag{8}$$

where ϕ stands for temperature/salinity and $(\partial\phi/\partial x) \approx ((\phi - \phi_{clim})/(\Delta x))$ during inflow.

Along with this set of boundary conditions, some of the prognostic variables are nudged to climatology

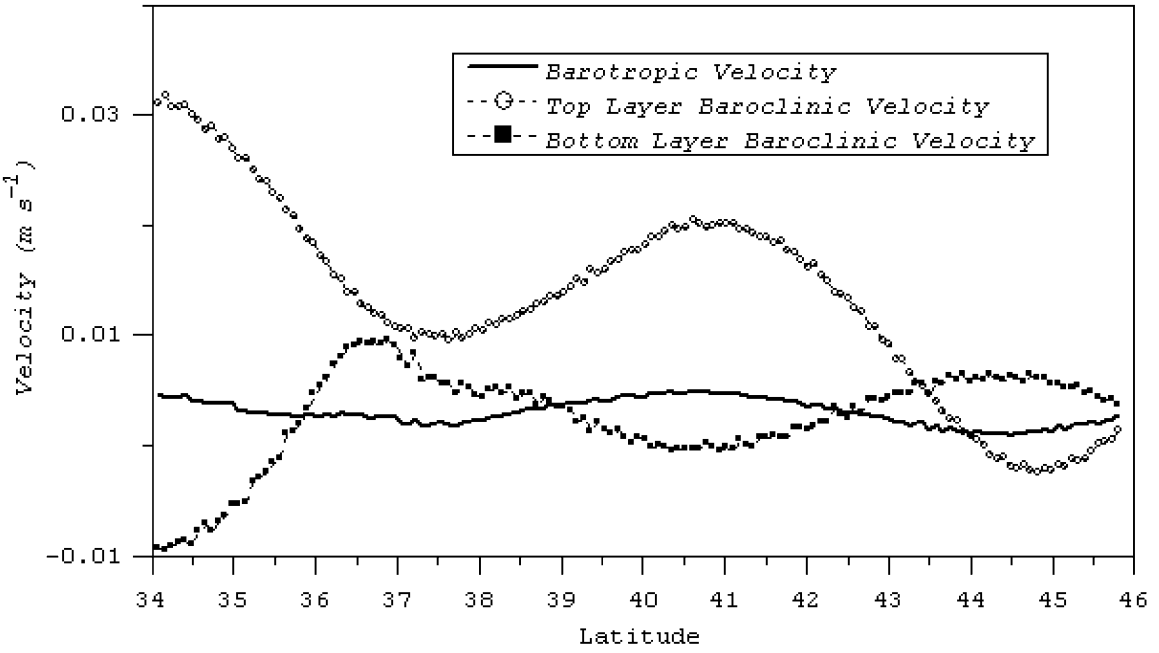

Fig. 2. Velocities applied at the western open boundary.

by applying a nudging term in the prognostic equations near the open boundaries:

$$\frac{\partial \phi}{\partial t} = \text{Advection} + \text{Diffusion} + \text{Sources} - \text{Sinks} + \frac{1}{\tau}(\phi - \phi_{\text{clim}}) \quad (9)$$

where ϕ stands for temperature, salinity barotropic and baroclinic components of velocity, τ is a relaxation time scale that varies smoothly from its value at the open boundary (180 days) to infinite within 100 km from the boundary. Finally, ϕ_{clim} is the external value computed from climatological data.

In order to implement the set of boundary conditions described above, we need to compute external values for the prognostics variables. For the scalars (temperature and salinity), the external data used is the same data used for model initialisation at the boundary points. The data is interpolated in time for the model time step allowing the boundary condition to be variable in time. To determine the barotropic velocities, a level of no motion at 2500 m is assumed according to Paillet and Mercier (1997) and Arhan et

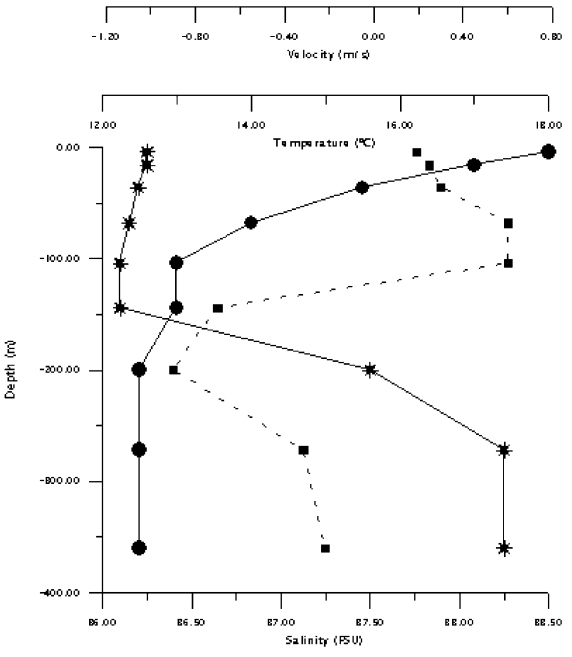

Fig. 3. Temperature (solid line + circles), salinity (solid line + asterisk) and velocity (dashed line + squares) imposed at the strait of Gibraltar.

al. (1994). Knowing the depth mean currents and the density field, we calculated the external baroclinic velocities normal to the boundary by assuming the thermal wind relation. Finally, since barotropic transports are known, sea surface height is calculated from the vertically integrated geostrophic relation. In Fig. 2, we show the velocities calculated at the open western boundary, where it is clear that the inflow is basically concentrated in two regions: south of 37°N where the Azores current flows to the east; and between 39°N and 42°N where the inflow is possibly associated with the recirculation of part of the North Atlantic Current to the south (Paillet and Mercier, 1997).

2.3. Experiment 1

In order to investigate the role of the meridional pressure gradient and its variable influence on the slope current along western Iberia, the model is initialised from rest with mean annual climatological temperature and salinity fields. It is then allowed to adjust to these fields in the absence of external forcing. The climatological temperature and salinity fields are extracted from Levitus and Boyer (1994) and Levitus et al. (1994) and are interpolated to the model grid before being smoothed using a simple cubic spline algorithm. In the upper 500 m, objectively analysed mean monthly temperature and salinity fields, estimated from CTD/XBT data supplied by the British Oceanographic Data Center (BODC), were used. This procedure provides a more detailed density field, which is very useful for describing the distribution of the meridional density gradient.

The model is run for 360 days; we assume the boundary condition at the Strait of Gibraltar to remain constant during this period (see Fig. 3). The values used at the Strait of Gibraltar are roughly the same as those used by Jungclaus and Mellor (2000). The volume transports specified are 0.8 Sv, both for inflow and outflow. The entrainment of North Atlantic Central Water in the Mediterranean Outflow that occurs in the Strait of Gibraltar is partially included since

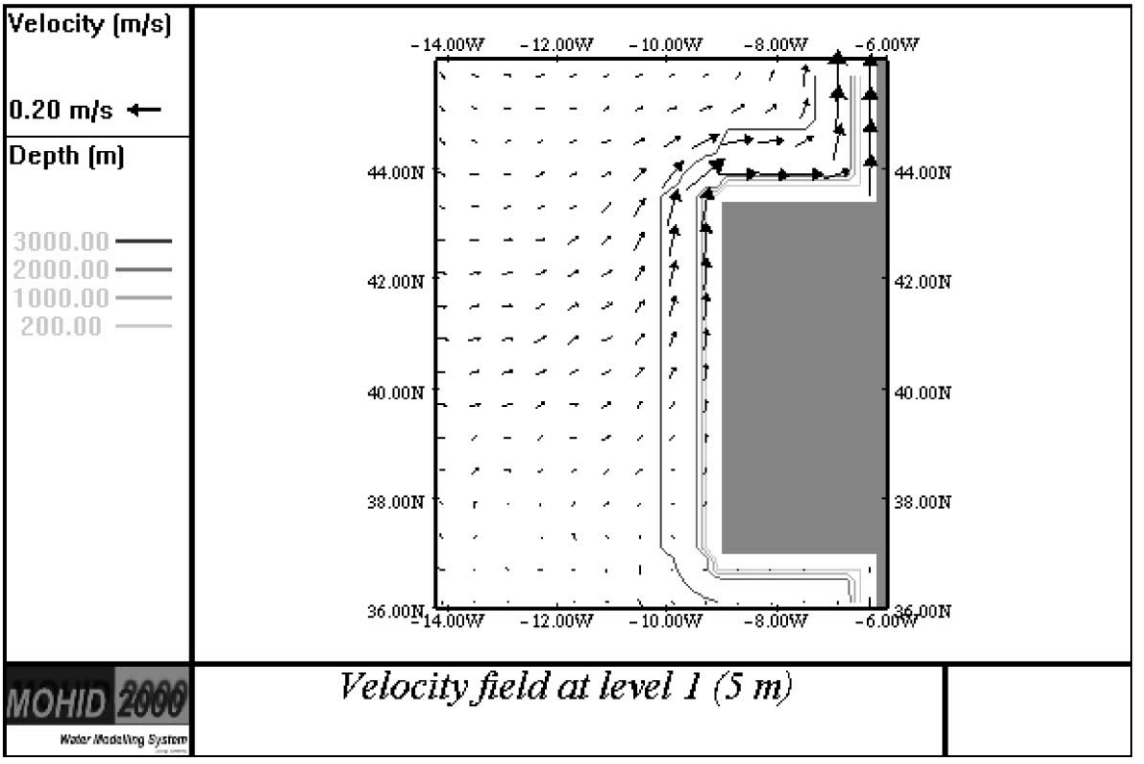

Fig. 4. Surface velocity field after 60 days. Bathymetry is superimposed with contours for 200, 1000, 2000 and 3000 m.

temperature and salinity are relaxed to its climatological values. The consequences of considering the boundary conditions constant in time at the Strait of Gibraltar are somewhat unknown. In fact, it is possible that the intermittency of the Mediterranean Outflow is at the origin of the formation of Meddies. Therefore, ignoring the variability of Mediterranean Outflow may have consequences for the simulated flow field along western Iberia.

2.4. Experiment 2

The model is initialised in the same way as in Experiment 1, but now using seasonal temperature and salinity fields. The spin-up phase consists of a 1-year run using monthly surface climatological momentum fluxes derived from the near-surface analyses of the European Center for Medium-Range Weather Forecasts ECMWF (Trenberth et al., 1990). After roughly 1 year, the volume-averaged kinetic energy is found to oscillate around an equilibrium value. Surface temperature and salinity are relaxed to climatological data during the spin-up phase. After this period, the model is run for 1 year using daily heat, mass and momentum fluxes from the ECWMF large-scale forecast model for the year of 1994. The spatial resolution of the ECWMF fluxes was $0.5 \times 0.5°$. The data is interpolated spatially for the model grid and temporally for the model time step. During the entire run, temperature and salinity are relaxed to climatological by adding an adjustment term $[-A(z)(\phi - \phi_{\text{clim}})]$ to the right hand side of scalar equations (ϕ being the temperature or salinity, ϕ_{clim} its climatological value and $A(z)$ given by $A(z) = 1/\tau[1 - \exp(z/\lambda)]$, with $\tau = 270$ days and $\lambda = 1000$ m).

The boundary conditions applied at the Strait of Gibraltar are the same as for Experiment 1.

3. Results from the model simulations

3.1. Experiment 1

This experiment was designed to investigate the role of the meridional pressure gradient in the generation of the slope current along the western Iberian Margin. An external pressure field may be the mechanism driving poleward currents along eastern ocean boundaries (Huthnance, 1984). Off Iberia, there is evidence of a maximum gradient in the sea surface slope at latitudes between 39°N and 41°N (Huthnance et al., 2002). This, together with complex topography—particularly Cabo da Roca, the Nazaré Canyon and the Galicia Bank—may induce meridional variability in the poleward flow. Existing theory and modelling studies have posited an increase of the slope current towards the north (Huthnance, 1984; Coelho et al., 1999). Fig. 4 shows a simulated meridional surface current for an idealized test case with a flat bottom at constant depth (4000 m), a slope and a shelf (200 m). Salinity was considered constant everywhere and the temperature was imposed using the annual mean along 12°W from Levitus and Boyer (1994), and was hence zonally uniform.

After 60 days, a poleward current developed over the slope/shelf break, increasing to the north. This

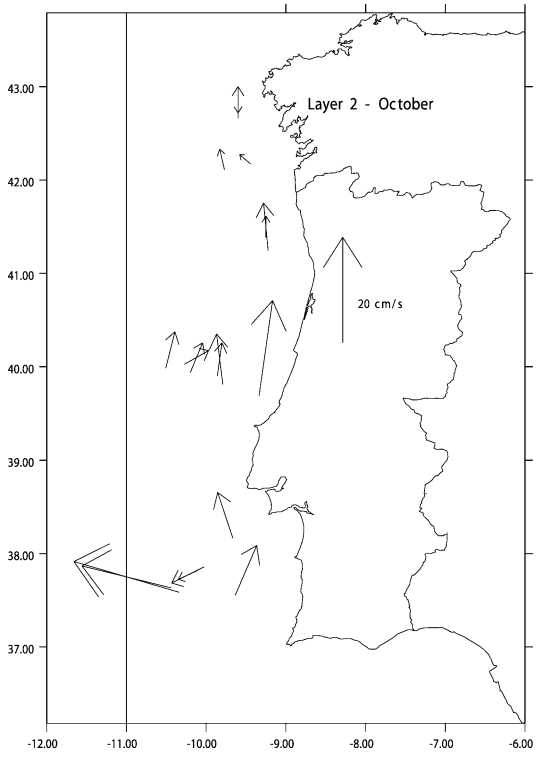

Fig. 5. Monthly mean currents recorded in October at depths between 200 and 800 m (Central Water). Data obtained during BORD-EST, MORENA, OMEX II–II and SEFOS and provided by the British Oceanographic Data Center (BODC).

result illustrates the typical solution expected for a current driven by the meridional pressure gradient. Mazé et al. (1997) have shown a different picture, however, from depth-integrated meridional transports. In the top 1500 m, they estimated transports, from the 1000 m isobath out to 10°W, of 8 and 4 Sv at 37.2°N and 43°N, respectively. Current meter analyses during OMEX II–II clearly show a northward decrease of the poleward slope current (see Huthnance et al., 2002; White, 1998). This poleward decline in slope current magnitude has been measured by Haynes and Barton (1990) and Fiúza et al. (1996). Analysis of archived current meter data has shown that the current reaches a maximum between Cabo da Roca and 41°N, before decreasing further north (see Fig. 5). It should be pointed out that even stronger poleward flows are observed to the south of Cabo da Roca, but here the variability of the flow is much larger and it is difficult to establish a consistent pattern for the flow. Further south, near Cabo São Vicente, Relvas (1999) observed

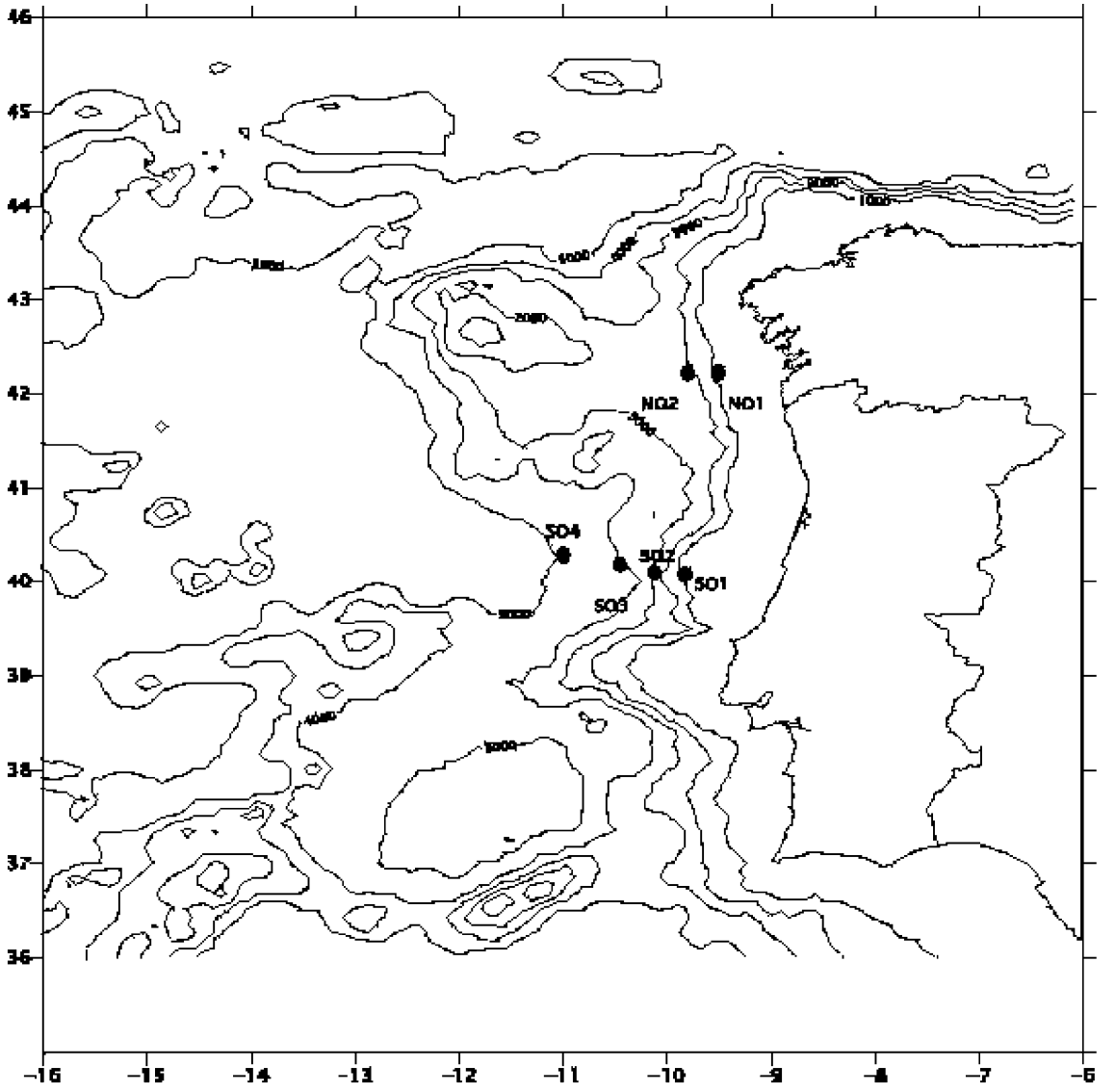

Fig. 6. Location of moorings used to estimate transports from current meter data and from model results.

a coastal surface poleward flow of up to 40 cm/s in the summer during an upwelling relaxation event, but it is not clear whether the mechanism underlying this poleward flow has any relation with the mechanism operating along the west coast. Similar results were shown by Mauritzen et al. (2001) using both an inverse model and ADCP data obtained during SEMANE95 (April 1995). These authors have suggested that the ENACW feeds the Mediterranean Outflow in the Gulf of Cadiz but also exhibits a westward recirculation within the shallow layers. Their estimate of transport within the Central Waters is about 1.7 Sv in a meridional cross section near Cabo São Vicente.

From the archived current meter data, we took two zonal lines to make a rough estimate of meridional transports. One of the lines is formed by the two inshore moorings in the northern position of BORDEST (Arhan et al., 1991), while the other one is formed by the two moorings from MORENA located at 42.218°N (see Fig. 6 and Table 1), hereafter designated sections SO and NO, respectively. Monthly volume transports were computed by integrating the spatially averaged velocity component normal to the section, between two depths and laterally between the moorings (Fig. 7). At first sight, these results might give the impression that they are in contradiction with Frouin et al. (1990) and with a very recent paper presented by Stevens et al. (2000), but this is not necessarily true. Their estimates indicate an increase in poleward transport in the upper 300 m from 0.13–0.3 to 0.37–0.5 Sv between 38°N and 42°N. Our analysis is based on current meter moorings with the uppermost current meter at depths of 300 m or more; it does not therefore give a very representative picture of the surface layer and consequently cannot be compared with the aforementioned results. Furthermore, the northernmost section that we are considering may not entirely catch the core of the poleward undercurrent, which would lead to an underestimation of the total transport. However, we believe that estimates using the current meter data can be used for comparison with model results.

Table 1
Location of current meters used to estimate fluxes

CM name	CM depth (m)	Local depth (m)	Latitude	Longitude
SO1_300	300	1171	40.08	−9.83
SO1_700	700	1171	40.08	−9.83
SO1_1000	1000	1171	40.08	−9.83
SO2_300	300	3838	40.1	−10.12
SO2_700	700	3838	40.1	−10.12
SO2_1000	1000	3838	40.1	−10.12
SO2_1500	1500	3838	40.1	−10.12
SO2_3000	3000	3838	40.1	−10.12
SO2_3600	3600	3838	40.1	−10.12
NO1_340	340	1338	42.218	−9.509
NO1_840	840	1338	42.218	−9.509
NO1_1240	1240	1338	42.218	−9.509
NO2_340	340	2337	42.218	−9.803
NO2_840	840	2337	42.218	−9.803
NO2_1240	1240	2337	42.218	−9.803
NO2_2040	2040	2337	42.218	−9.803

Clearly, the transports are more intense in the southern section. In both sections, we found the same seasonal pattern with the transports decreasing to a minimum value in July and then increasing again to a relative maximum in September (comparable to the values obtained for May). In the southern sections, the contributions from the layers corresponding to Central Water and Mediterranean Water are comparable. However, in the northern section, the contribution from the layer between 450 and 900 m is dominant, except in September/October, when it is comparable to the contribution from the layer located between 1000 and 1300 m.

We also used the CTD data collected by OMEX during Winter 1997 to compute geostrophic transport (for 1250 dbar) at 42°N and 43°N. Our estimates indicate 1.73 Sv (at 42°N) and 1.31 Sv (at 43°N) at Central Water levels and 0.64 Sv (at 42°N) and 0.42 Sv (at 43°N) at Mediterranean Water levels. Further transport estimates are presented in Huthnance et al. (2002).

We also performed runs using the density fields for Autumn, Winter, Spring and July (not shown), in addition to the experiment described above with mean annual data. In general, flow structures in all runs were comparable, although some differences are found in terms of current intensity and associated transport. This was not surprising since calculations of volume transports associated with the large-scale meridional pressure gradient in the North Atlantic suggest that it is present all year round and weakens during summer (Klein and Siedler, 1989). The large-scale eastward flow generated by this meridional pressure gradient occurs in the upper 200–300 m; near the eastern ocean boundary, this flow forces coastal downwelling and a resultant surface poleward current. This flow charac-

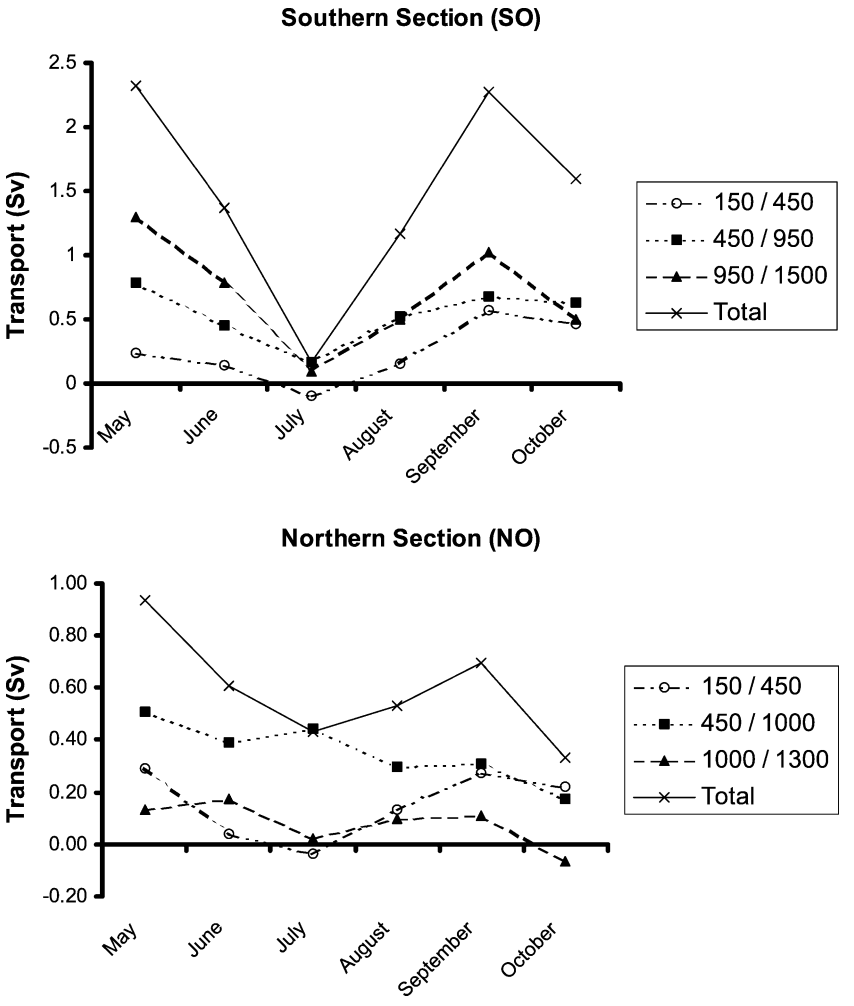

Fig. 7. Meridional transports estimated from current meter data for the zonal sections formed by moorings SO1 + SO2 (top) and NO1 + NO2 (bottom) — see also Fig. 5. Numbers in the key refer to depths used for integration.

teristic at an eastern boundary has been corroborated in model results obtained by McCreary et al. (1986) and Weaver and Middleton (1990) for the Leeuwin Current.

The average velocity field at 5 m depth in northwestern Iberia for the last 30 days of the run is shown in Fig. 8. On the shelf/slope, a poleward flow was present, the result of coastal adjustment to the oceanic eastward flow. Currents are strongest between Cabo da Roca and 41 °N and decrease to the north. To the south of 39 °N (not shown in Fig. 8), currents are relatively strong but the flow is more complex. Offshore, west of 10 °W, the general equatorward flow of the subtropical gyre was found. The width (about 50 km) and intensity of the poleward slope current were comparable to previous observations and previous model results (e.g. Stevens et al., 2000, Fig. 5) except over the shelf. This is due to the absence of wind — the dominant mechanism in these waters — from our experiments. Nearing 41 °N, a large portion of the poleward slope current is deflected offshore. Part of this flow recirculates to the north around the Galicia Bank, confirming the picture suggested by Mazé et al. (1997). A smaller portion turns south forming a cyclonic eddy centred at nearly 40.5 °N and 11 °W. Near Cape Finisterre, the poleward slope current becomes narrower and stron-

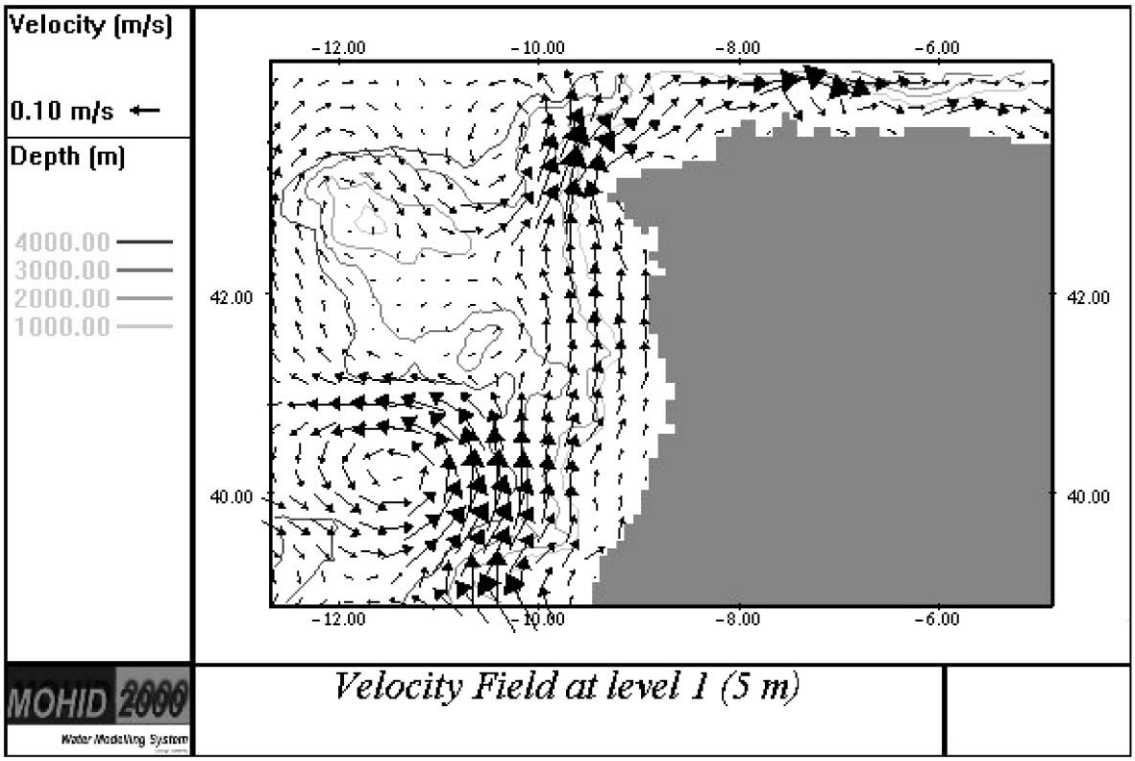

Fig. 8. Zoom of velocity field at level 1 (5 m) at day 90 for northwest Iberia. To avoid clutter, the velocity vectors are plotted every second grid point in both directions.

ger, partially incorporating part of the flow that has recirculated around the Galicia Bank. The interaction of the eastward slope current with the westward current found offshore to the north gives rise to the formation of cyclonic eddies typical of this region (Dubert, personal communication).

The transports computed by the model at the sections shown in Fig. 5 are shown in Fig. 9 together with other independent transport estimates. The total transport in section SO is 2.5 Sv, distributed vertically as follows: 0.8 Sv in the upper 400 m, 1.6 Sv between 400 and 900 m and 0.1 Sv between 900 and 1500 m. At the northernmost section, the total transport is 0.9 Sv, 0.7 Sv between 400 and 900 m and 0.2 Sv in the upper layer.

Monthly current stability R, defined as $R = |\overrightarrow{\overline{v}}| / |\overrightarrow{\overline{v}}|$, was computed for the current meter data available. It was found that R increases with the magnitude of the mean monthly current vector. Monthly variation in current stability may reflect a balance or domination of one of the forcing processes: wind and the meridional pressure gradient. Values for R are higher in the intermediate waters, particularly at MW levels. In the upper layers, over the shelf/slope regions, peaks in R were found in July, October and December, with minimums in early summer and spring. The minimums may reflect a period of transition between the two dominant forcing mechanisms. At times when one forcing mechanism is dominant, e.g. in July (upwelling) or December (density driven flow) we can expect higher R values, as measured. It was for the months of May and September/October that the closest agreement between observed and model fluxes at lines SO and NO was found. This may indicate that at this time of the year, the flow was mainly driven by the meridional pressure gradient. If this is the case, then we can conclude that the model is producing very reasonable results.

In Fig. 9, we compare the model results at sections NO and SO with transports calculated from current

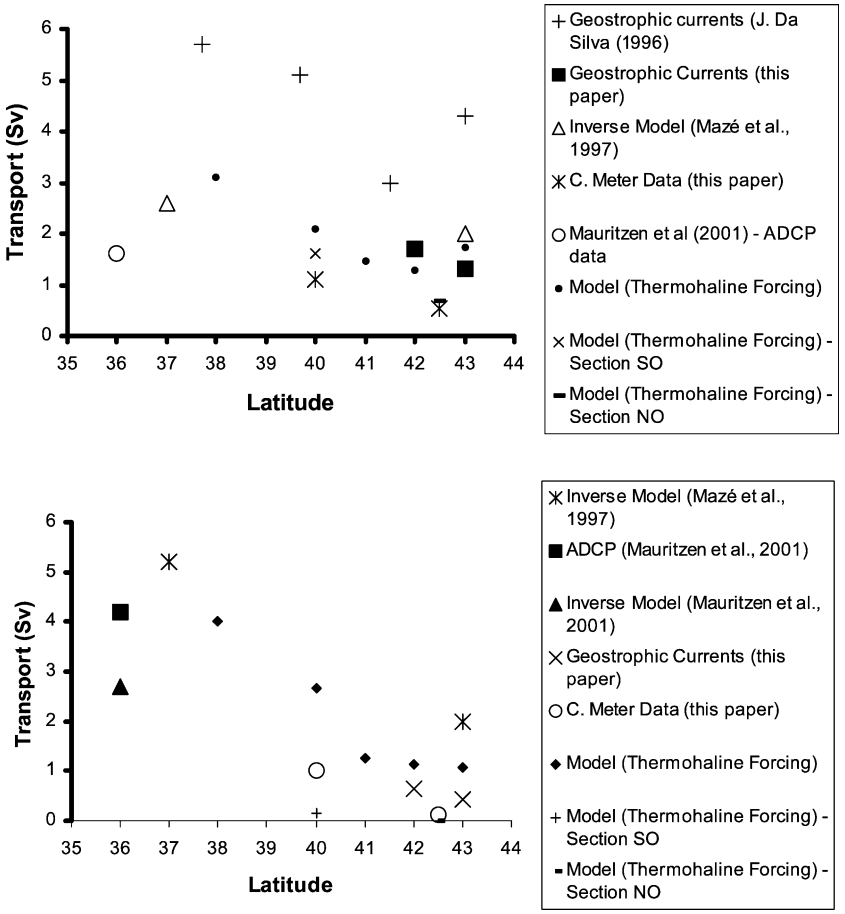

Fig. 9. Estimated poleward transports along the Iberian Margin. In the top panel are represented transports estimated within North Atlantic Central Waters while in the bottom panel are the transports within Mediterranean Waters. The current meter data used for estimation of transports is relative to May. The data from Mauritzen et al. (2001) was obtained in the southern coast of Portugal.

meter data for May. The transports calculated with the model at sections NO and SO lend some plausibility to the results, but further insight into the meridional structure of the slope current is not possible by analysing these sections alone. Therefore, we measured transports in other sections along western Iberia. An isobath that roughly followed the western limit of the slope current was chosen and transports estimated between that isobath and the shelf. From current meter data at line SO, it was possible to conclude that the 4000 m isobath basically corresponds to that limit. Between 38°N and 41°N, the 4000 m isobath is located very near to 10.5°W. At 42°N and 43°N, the presence of the Galicia Bank pushes the 4000 m isobath to the west. As we are interested in what is happening close to the slope and, especially, in the exchange between shelf/slope and the deep ocean, we preferred to compute meridional fluxes in consecutive sections (at 38°N, 40°N, 41°N, 42°N and 43°N) between 10.5°W and the shelf. The fluxes calculated in the top 1500 m are also shown in Fig. 9. The results demonstrate that transport is not increasing northward. The highest values were found at 38°N, but at 40°N, transport is reduced by 25%. The reduction is particularly evident at Mediterranean Water levels. This agrees very well with Daniault et al. (1994) and Mazé et al. (1997), who proposed that part of the MW that is flowing northward along the southern Portuguese slope is deflected to northwest and possibly to the west when it reaches the Tagus Basin. From 40°N to

41°N, there is a small decrease in transport but velocities close to the slope increase at these latitudes. The decrease in transport might be explained again by deflection to the west due to the presence of the Vigo Seamount. The increase in velocity probably reflects the reduction of the sectional area enclosed between the 3000 m isobath and the shelf. At 42°N, velocities and transports are lower than at 41°N. Here the reduction of velocities and transports is a reflection of the increase of the section between the 3000 m isobath and the shelf—this area is a wide valley enclosed between the shelf and the Galicia Bank—and especially the recirculation of the slope current around the Galicia Bank. The relatively small decrease in transport may be explained by the fact that the meridional pressure gradient is concentrated between 39°N and 41°N and is contributing to increase the slope current meridional transport in the absence of topographic obstacles. Finally, between 42°N and 43°N—the area of interest for OMEX—meridional transport is slightly increased, reflecting the partial "return" of the slope current recirculating around the Galicia Bank.

3.2. Experiment 2

The major objective of this experiment was to simulate the flow under more realistic forcing con-

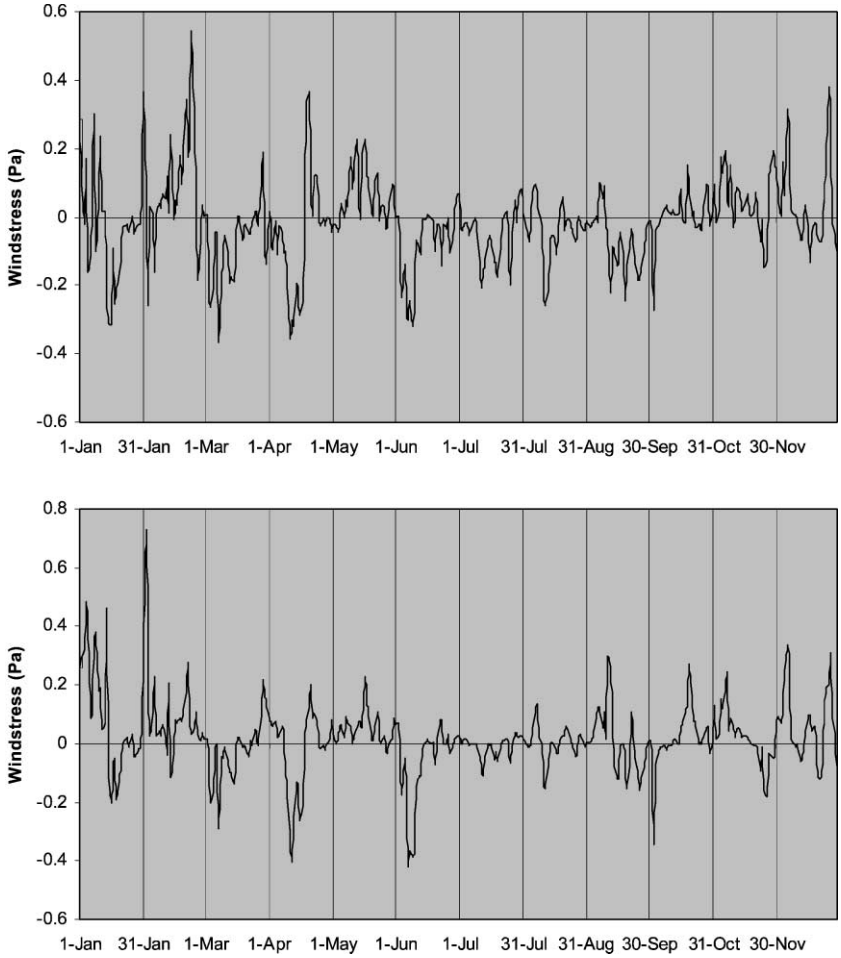

Fig. 10. Meridional (upper) and zonal (lower) components of windstress at 42.5°N.

ditions. To achieve this goal, realistic daily winds for the year of 1994 were used. We chose 1994 because several long-term current measurements are available for this year. Fig. 10 illustrates the variability of the meridional and zonal components of windstress at 42.5°N. The upwelling season—associated with negative values of the meridional component of windstress—starts in June with a very strong event and ends at the beginning of September. It can be seen that during the winter—from January to March—there were several events of upwelling-favourable winds. From late summer to December, winds were weaker than in summer and consistently from west/southwest. With this pattern for windstress, we expect to be able to reproduce the seasonal variability of the flow off the Iberian Peninsula. Fig. 11 shows average surface flow for February. We chose this month as one in which the winds were strong and predominantly from the west/southwest, with an upwelling event towards the end of the month. The model response to the winds includes the surface poleward current that, at 40°N, extends from the shelf to 11°W with a maximum value of 15 cm/s over the slope (1000 m isobath). At 42°N, the maximum surface current over the slope has decreased to approximately 5 cm/s, thus comparing very well with the 3.9 cm/s of monthly mean current observed at 56 m depth for the same period at 42.267°N, 10.15°W (see Table 2 for a summary of observed currents during February 1994). Below the surface layer, a poleward undercurrent was present. Near 42°N, at MW levels, the model produces poleward currents of about 2 cm/s that are two or three times lower than those observed (see Fig. 12). The circulation obtained at 1040 m was very similar to that presented by Stevens et al. (2000)—Fig. 7b in their paper—for May. In particular, it should be pointed out that in their model, poleward flow at these depths almost vanishes at 42°N. This agrees with results obtained with drifting buoys at 1500 dbar in the ARCANE project, which

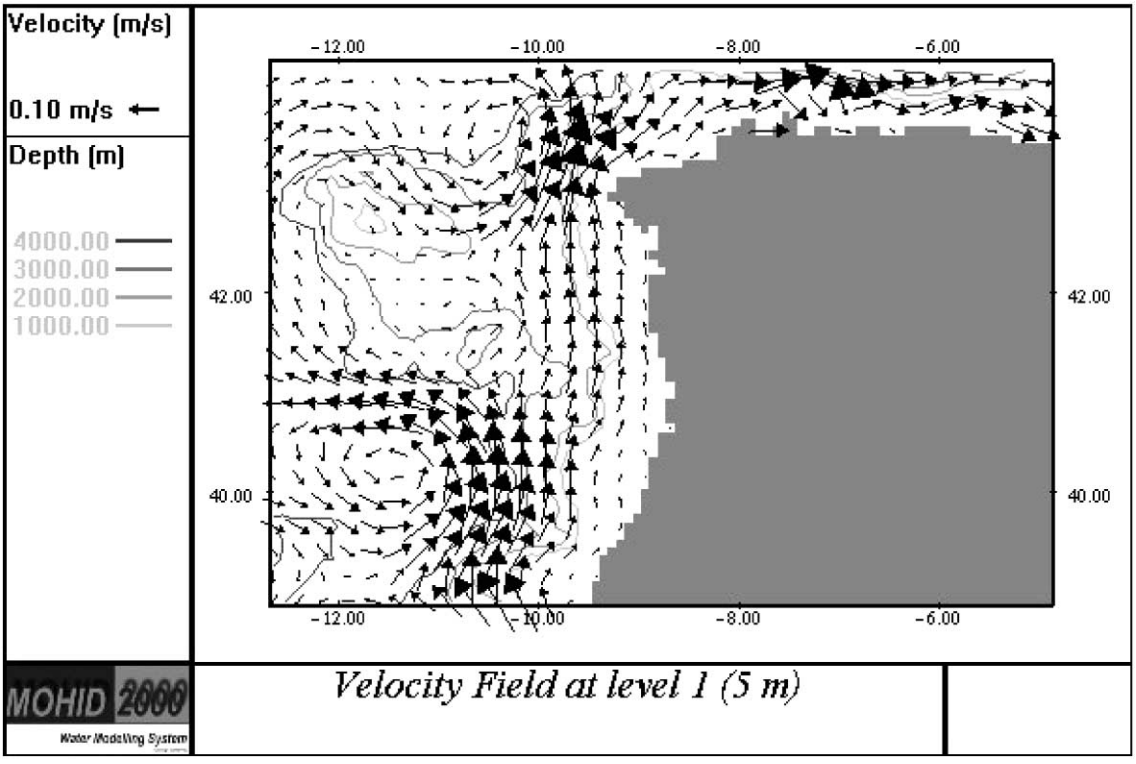

Fig. 11. Zoom of monthly averaged velocity field at level 1 (5 m) for February 1994. To avoid clutter, the velocity vectors are plotted every second grid point in both directions.

Table 2
Statistics for current meters located between 42°N and 43°N in February 1994

Latitude	Longitude	Depth	CM depth	East velocity (cm/s)	North velocity (cm/s)	Stability
42.267	− 10.15	2700	2000	0.64	5.86	0.97
42.267	− 10.15	2700	256	− 1.83	3.41	0.72
42.267	− 10.15	2700	56	− 0.52	3.92	0.62
42.267	− 10.15	2700	756	− 0.53	2.69	0.95
42.267	− 10.15	2700	1156	− 0.66	6.74	0.98

give some indication of a southward flow at these latitudes. Moreover, the geostrophic velocities derived from hydrographic data collected during the MORENA 1 cruise (Fiúza et al., 1998) only show northward flow very close to the continental slope (as in the model). A well-established poleward current is only seen to the south of 41.5°N. According to the same authors, maximum salinity was found to be at 1150 dbar at 40°N and at 1050 dbar or even less near 43°N. It is possible that the presence of low-salinity Atlantic Waters on the northern part of the Iberian margin (forming the so-called Galicia Front) restrict the lower core of Mediterranean Water to the vicinity of the slope off Cape Finisterre. It is also possible that the model is underestimating the poleward flow at these levels. We will return to this subject later in this paper.

By the end of February, wind direction veered suddenly from southwesterly to northerly. In Fig. 13, we show the surface velocity field on 28 February 1994. In the top layer (5 m depth), the current is still poleward over the shelf break/slope. Further to the east and over the shelf, however, the current is now res-

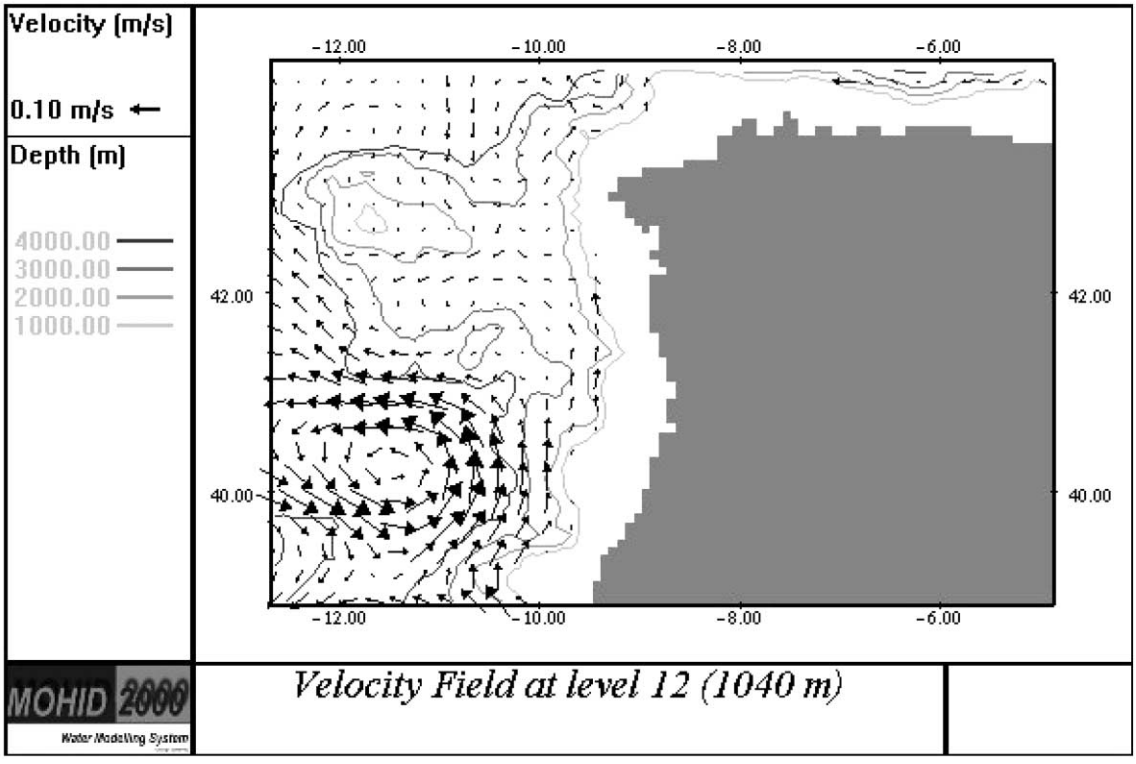

Fig. 12. Zoom of monthly averaged velocity field at level 12 (1040 m) for February 1994. To avoid clutter, the velocity vectors are plotted every second grid point in both directions.

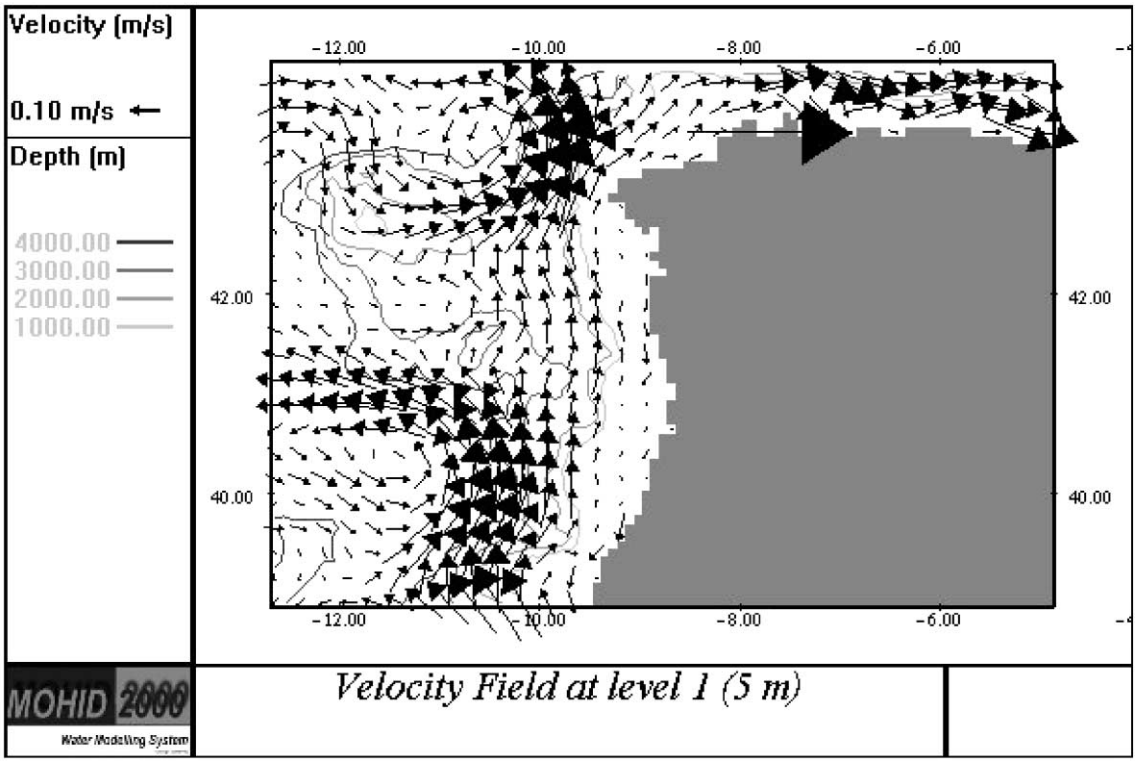

Fig. 13. Zoom of velocity field at level 1 (5 m) on 28 February 1994. To avoid clutter, the velocity vectors are plotted every second grid point in both directions.

ponding to the winds becoming prevalent from upwelling events. To the west, circulation does not depart too much from the average. This kind of event is very difficult to distinguish in satellite images since the upper ocean is very well mixed at this time of the year and consequently the thermal signature cannot be seen. Over the shelf, on the other hand, it is very common to find cool and fresh water originating from river runoff, which also hinders the identification of upwelling patterns. In terms of water fluxes, the scenario is not very different from what we presented in the previous section (see Fig. 14). At 38°N, the major differences were found in the top layer, where transport in February is slightly higher in comparison with the results of Experiment 1. At Mediterranean Water levels, transport also increased, contributing to a total transport (in the upper 1500 m) in excess of 8 Sv between 10.5°W and the coast. At 40°N, transport was again lower than at 38°N, but higher than results from thermohaline-driven circulation. At 41°N, total transport is 2.5 Sv, which is comparable with previous results. At 42°N and 43°N, the transports calculated are lower than in Experiment 1. The major factor in this decrease at 42°N was located at MW level, since—as mentioned above—the current almost vanished. Finally, at 43°N, transport is slightly increased. Looking carefully to the vertical structure of the transports, we have found that at the upper levels, there was an increase of 1.1 Sv between 42°N and 43°N and a decrease of 0.8 Sv in the Mediterranean Water layer (750–1500 m). This is an indication that circulation was onshore in the upper layers and offshore below (see also Figs. 11 and 12), with the onshore circulation and the consequent increase in transport probably due to wind forcing and the "return" of the slope current to north of the Galicia Bank. However, we should note that onshore Ekman transport, according to Huthnance et al. (2002), is 0.05 Sv, and therefore does not fully account for either the total amount of water entering at 10.5°W or the higher transport at 43°N by comparison with Experiment 1.

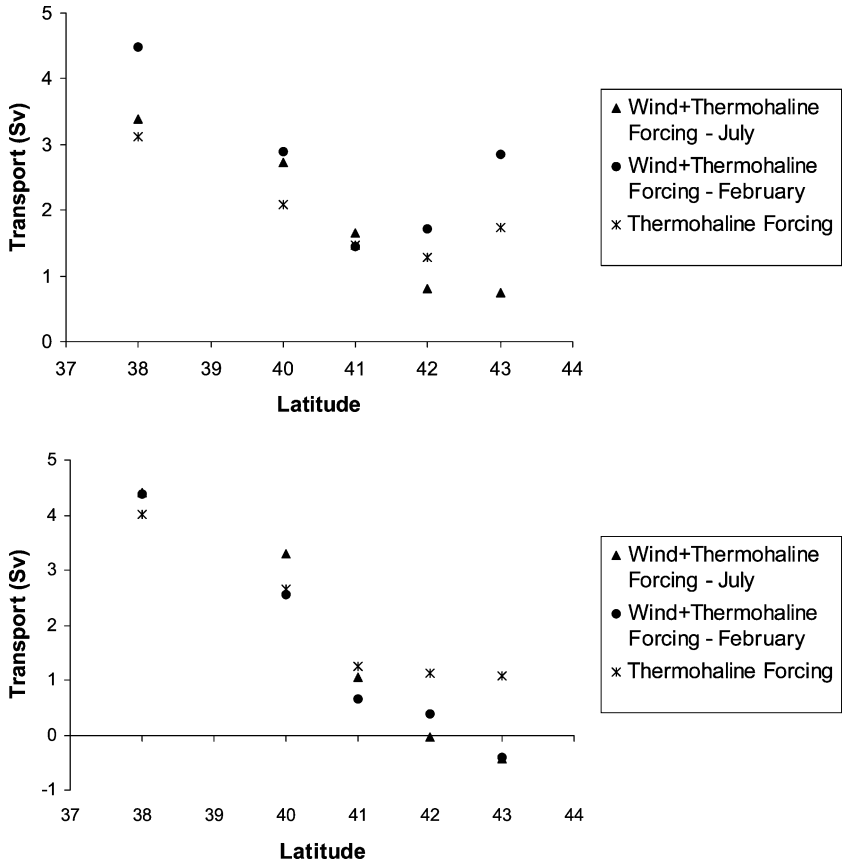

Fig. 14. Meridional transports along the Iberian Margin estimated with the model. In the top panel are represented transports estimated within North Atlantic Central Waters while in the bottom panel are the transports within Mediterranean Waters. The results obtained in Experiment 1 are repeated here for purposes of comparison.

The tendency for export to deep ocean at intermediate levels is confirmed by current meter data. In fact, most of the 13 readings obtained in CW and MW between 42°N and 43°N revealed westward flow with values ranging from 0.4 to 2.2 cm/s (see Huthnance et al., 2002). The same can be observed for this particular month of February 1994 (see Table 2).

July was chosen to illustrate typical summer circulation, as during this month, the winds were predominantly from the north (Table 3). The average surface velocity field is shown in Fig. 15, revealing an equatorward flow over the shelf that reaches 10 cm/s. Further to the west, over the slope, the flow was poleward with relatively high velocities due west from Lisbon. Similar poleward flows were obtained using models by Stevens et al. (2000) and during the DYNAMO project. Stevens et al. (2000) attributed this poleward flow to the climatological nature of the forcing since MORENA cruises have shown equatorward rather than poleward flow. In our model, the wind forcing was more realistic, thus climatological factors cannot be invoked. Instead, we argue that 1994 was not a year particularly favourable for upwelling occurrence, with monthly average values for the upwelling index at 42°N generally lower than 30 m^3 (100 m^{-1})—the exception is July with a value of 77 m^3 (100 m^{-1}). Furthermore, upwelling started in June, which is relatively late compared with other years, when it starts in April/May. This means that the poleward flow in July 1994 may be a remnant of the winter surface poleward current. One further explanation for the poleward flow over the slope may be

Table 3
Statistics for current meters located between 42°N and 43°N in July 1994

Latitude	Longitude	Depth	CM depth	East velocity (cm/s)	North velocity (cm/s)	Stability
42.218	− 9.803	2337	2037	− 0.01	− 048	0.47
42.218	− 9.803	2337	837	− 1.95	0.58	0.65
42.218	− 9.803	2337	1237	− 1.29	0.54	0.45
42.218	− 9.803	2337	337	0.51	− 2.54	0.81
42.267	− 9.509	1338	1238	0.43	0.09	0.44
42.218	− 9.509	1338	338	0.79	1.59	0.53
42.218	− 9.509	1338	838	− 096	5.58	0.98

windstress curl. Lopes da Costa (1991), using a 3D model developed by Haney (1985) and modified by Batteen et al. (1989), concluded that a large negative windstress curl (between 48 and 64 km from the coast) followed by a positive windstress curl (between 64 and 182 km) leads to the formation of a southward surface coastal current, followed offshore by a surface poleward current with velocities up to 40 cm/s, a width of 120 km and a vertical extension of 560 m. The equatorward surface current nearshore and the offshore poleward current were shown to be approximately in geostrophic balance with the pressure gradient forces due to horizontal distribution of density. McCreary et al. (1987) proposed a similar mechanism for the Davidson Current. The maps proposed by Bakun and Nelson (1991) show that the windstress curl for Iberia is positive. Finally, we analysed the windstress curl distribution for Iberia during the

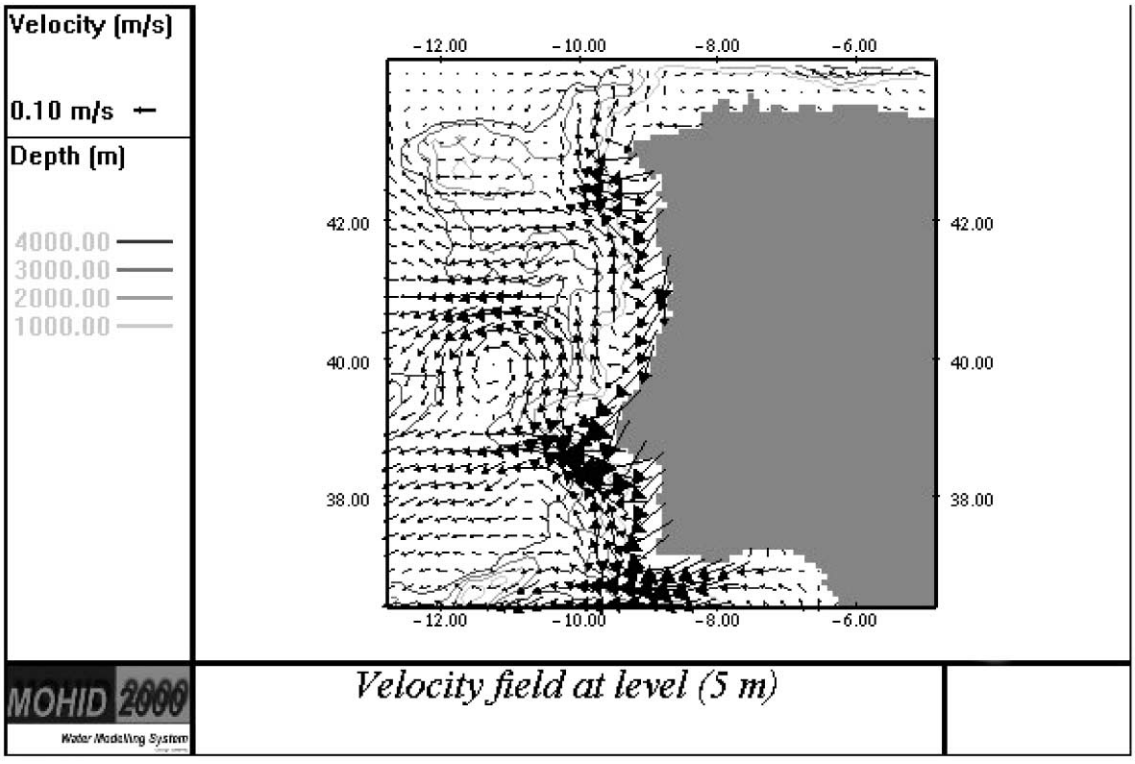

Fig. 15. Zoom of monthly averaged velocity field at level 1 (5 m) for July 1994. To avoid clutter, the velocity vectors are plotted every second grid point in both directions.

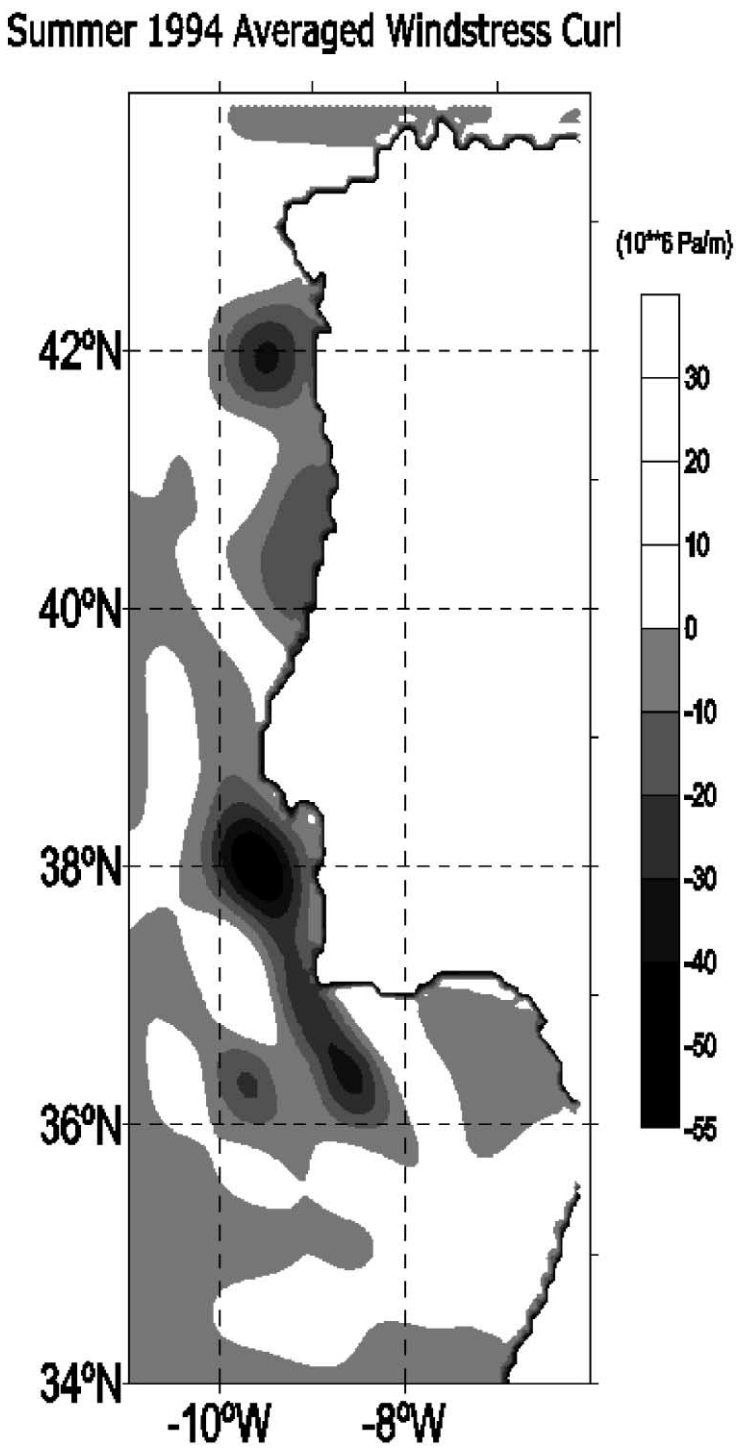

Fig. 16. Averaged distribution of windstress curl for the summer 1994.

summer of 1994. Fig. 16 shows that there is a band of positive windstress curl particularly in evidence to the north of Cabo da Roca, and this may be driving the poleward current offshore. Unfortunately, there is no current meter data available for surface layers to compare with the model. We should point out that in August and September, the circulation is very similar to that presented in Fig. 15.

At MW levels, circulation was very similar to that shown in Fig. 17 for February, confirming that the slope undercurrent is present all year round. The surface temperature pattern (Fig. 17) shows a difference of 3 °C between coastal and outer slope waters, which is comparable with results obtained by Stevens et al. (2000) and the DYNAMO project. Turning back to meridional transports — shown in Fig. 14 — model results indicated that the total transport in the upper 1500 m was poleward at all sections, relatively small when compared to February, but with the same structure as described above. At the OMEX box, the meridional transport has diminished from 42°N to 43°N between the surface and 750 m, indicating that the cross-slope exchange is towards the open ocean. The amount of water exported was about 0.1 Sv. A closer look to transports crossing a smaller box with a western limit at the shelf break gave, at 43°N, a southward flux of 0.14 Sv that fell to 0.1 Sv at 42°N. The westward flux crossing the shelf break was estimated to be 0.05 Sv.

3.2.1. Vertical structure

Fig. 18 illustrates the vertical structure along a zonal section located at 40°N at the end of July 1994. The current has a surface maximum over the 600 m isobath and a subsurface maximum at the level of the upper Mediterranean Water core. Comparison of these results with Fig. 6 of Stevens et al. (2000) indicated that our poleward current was more confined to the slope (generally eastward of 10°W) and five to six times more intense. Computed velocities, however, were similar to Fig. 11b from Daniault et al. (1994),

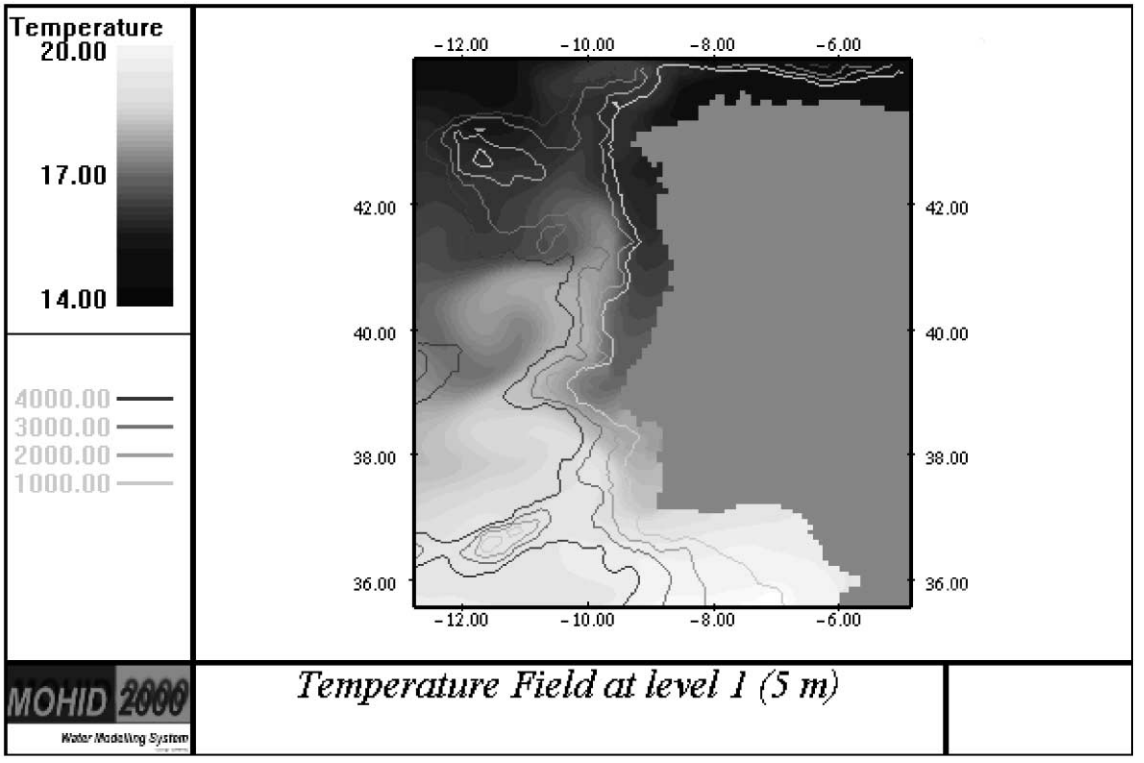

Fig. 17. Zoom of surface temperature (5 m) at the end of July 1994.

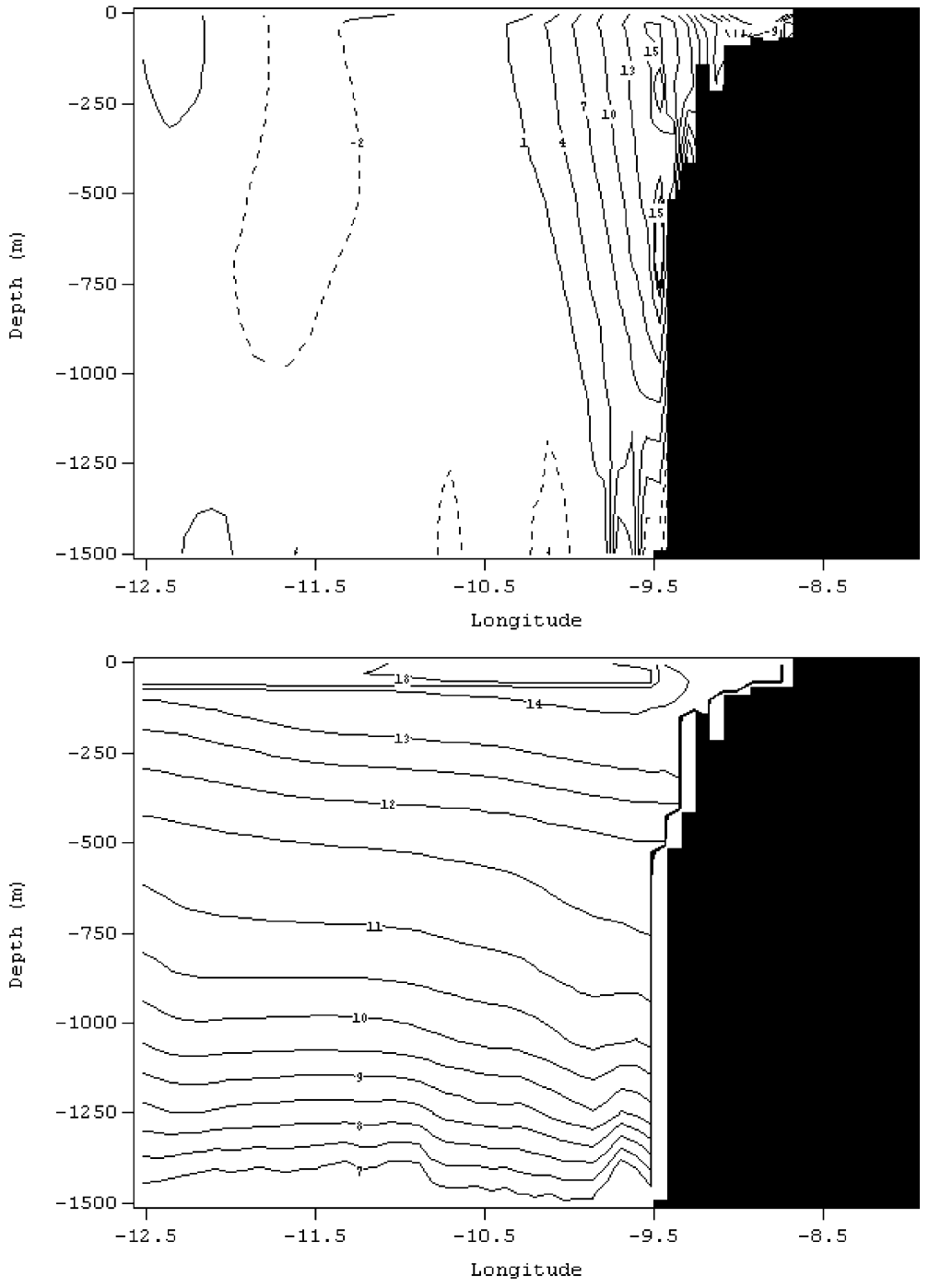

Fig. 18. Zonal sections of meridional velocity (upper panel), temperature (lower panel) and salinity (next page) at 40°N at the end of July 1994. Velocity is in cm/s.

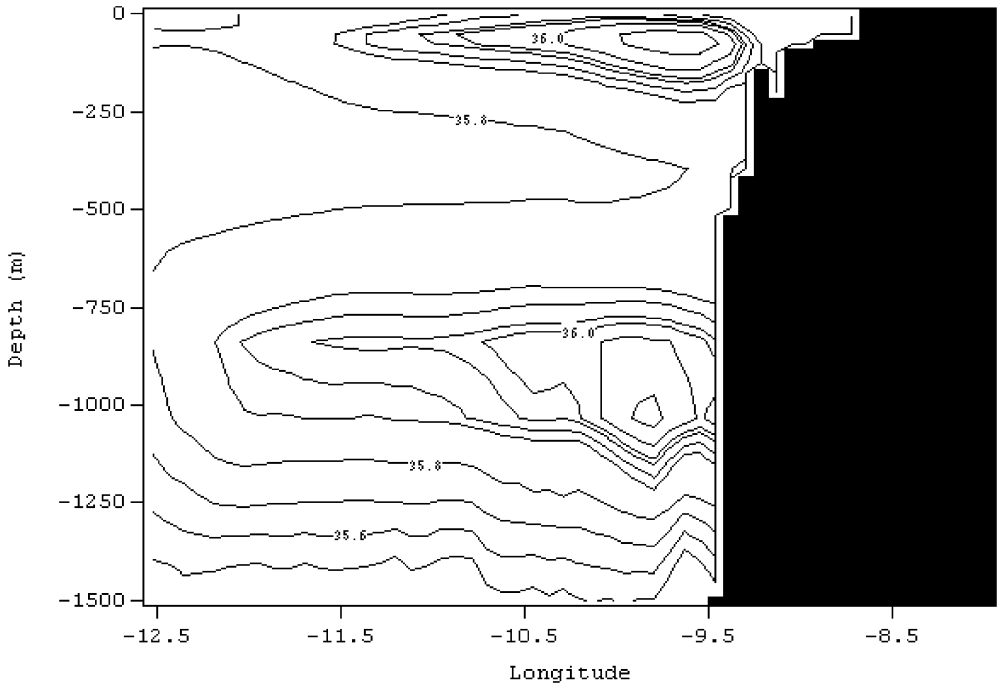

Fig. 18 (*continued*).

which indicated geostrophic velocity at 40°N. The barotropic nature of the flow away from the slope was in agreement with the conclusions drawn by Fiúza et al. (1996) based on current meter data obtained during MORENA at approximately 41°N and 42°N. Close to the slope, the current records the two maximums enhancing a more baroclinic structure. We also analysed the currents in the moorings SO1 and SO2 and concluded that at SO2 (offshore), the first mode of variability (the barotropic one) explained 71% of the total variance, while at SO1, only 54% of the variance was explained by that mode. Salinity and temperature sections highlighted the existence of the two cores of MW. The upper core was seen as a temperature maximum near 650–750 m with a value of 11.75 °C at 40°N and less than 11.5 °C at 41°N (not shown), indicating the poleward decrease due to both vertical and horizontal mixing. The upper core of MW was previously identified by Zenk and Armi (1990) and, more recently, during MORENA, by Fiúza et al. (1998). The lower core of MW can be seen in Fig. 18 by the salinity maximum centered at 1000 m and the salinity field at 1040 m illustrating the spreading of MW in the model domain (Fig. 19). There is remarkable agreement in the distribution pattern with Fig. 4 from Daniault et al. (1994), even if the model values are lower than those observed. There are several possible explanations for the lower salinity values obtained for these latitudes by the model. Numerical diffusion due to the advective scheme is one possible reason for the lower values of salinity in the northern part of the domain. On the other hand, it is well known that *z*-level models present vertical overmixing that may also contribute to the reduction of salinity. Finally, there is some reason to believe that the entrainment of Central Water at the Gulf of Cadiz is underestimated, resulting in an excess of recirculation at Central Water levels and consequently transports that are higher than those observed, while at Mediterranean Water levels, transports are lower.

In a sense, it is rather surprising that total transport in all the cross sections along western Iberia defined between 10.5°W and the coast was poleward. However, the results presented by Mazé et al. (1997)

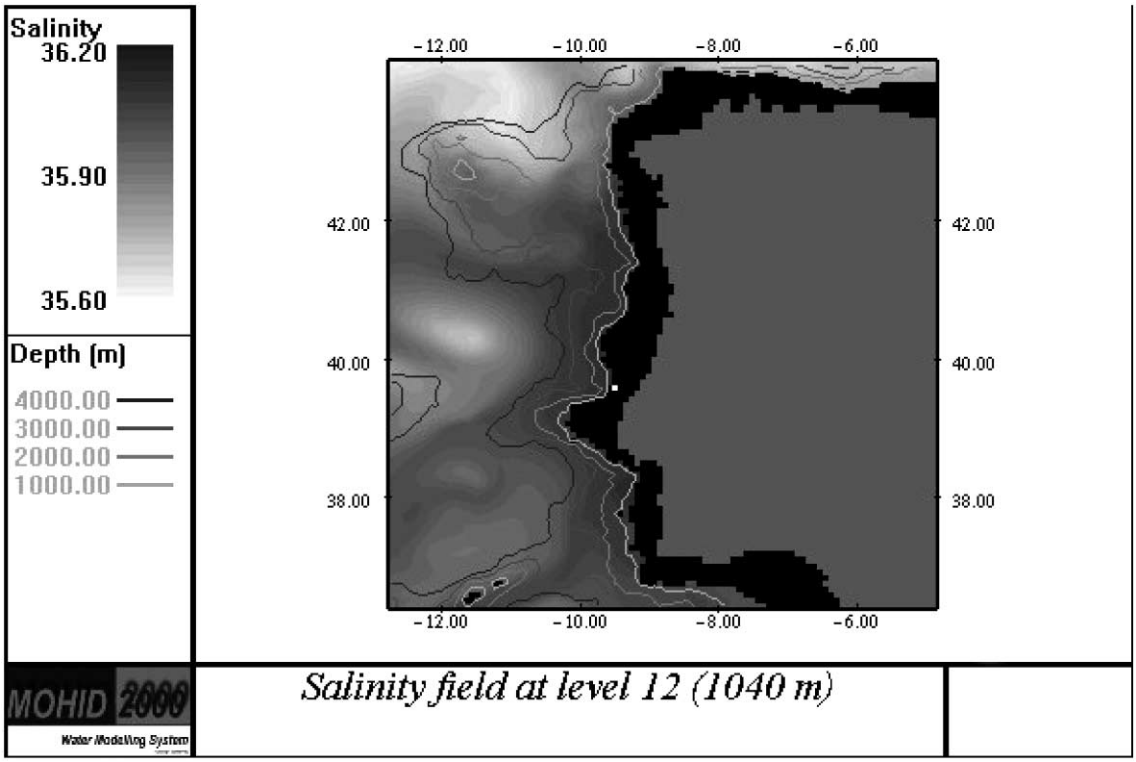

Fig. 19. Salinity field at level 12 (1040 m) at day 90 — dark grey stands for higher salinities. Depth contours are represented.

suggested the same pattern. In the same paper, the authors studied what they call the *modified solution* that they considered to be more representative of upwelling conditions; the conclusion was the same, even if transports to the north were much reduced in this case. These model results, as well as others presented by Stevens et al. (2000) and by the DYNAMO group (Barnard et al., 1997), have shown this same tendency under different forcing conditions. ADCP data from Relvas (1999) obtained in an expedition during the upwelling season also revealed a well-established poleward flow at 37.5°N, extending from the surface down to 450 m and located to the west of 9.8°W. The intensity of the meridional velocity was 10 cm/s near the surface. Further to the south, the currents were even more intense (20 cm/s at 37°N). The hydrological structure observed during the expedition was consistent with the velocity measured, thus excluding the possibility of these currents being related with the tide. This is a subject that clearly needs clarification in the future.

4. Conclusions

We applied a three-dimensional model to the west coast of Iberia with the aim of investigating the role of thermohaline and wind forcing in circulation. The results were compared with available data and previous studies on circulation in the area. The model succeeded in reproducing the general patterns of circulation as well as seasonal variance.

Transports were predominantly along-slope, and especially so in the OMEX box. However, the total amount of water exported from the shelf/slope to the deep ocean along the west coast of Iberia was relatively high (4–6 Sv). The exchange occurs essentially at Mediterranean Water levels and seems to have preferential locations, since most of the cross-slope transport occurred between 38°N and 40°N (the role of the canyons of Nazaré and Setúbal is not clear here, but it is possibly very important and deserves closer examination in the future). This further illustrates the need to look at the OMEX fluxes for the whole Iberian

Margin, as proposed by Huthnance et al. (2002), instead of considering only the OMEX box. Finally, we should point out that filaments of cold water during the upwelling season may contribute significantly to cross-slope exchange (Huthnance et al., 2002). However, to generate filaments in the model, we need very high resolution (2 km). We also need to cover a very large area to obtain a good overview of large-scale circulation, something that is not compatible with the resolution needed to simulate filaments.

Two other major findings of this modelling were: (1) integrated transport in the upper 1500 m between 10.5°W and the coast was always poleward for the forcing conditions considered in this study; and (2) transport decreased further north, in apparent close correlation with topography. This observation seems to be supported by current meter data and by previous studies (Mazé et al., 1997). Stevens et al. (2000) wrote that "the surface poleward current [...] rather than being a winter feature it was a non-summer feature". Our results indicate that the surface poleward current over the slope was a permanent feature, at least for 1994. However, this was a year with a low upwelling index in the summer months and it may be viewed as anomalous. It is tempting to hypothesize that: (1) the surface poleward current is always present as long as the meridional component of windstress is not strong enough to revert the flow; and (2) the reversal of the flow occurs over the shelf first, and may not occur over the slope.

To gain a more realistic picture of circulation and fluxes off the Iberian peninsula, we need to improve horizontal resolution so that filaments can be simulated. Other possible improvements are: (1) to take river runoff (which is not negligible, according to Huthnance et al., 2002) into account; (2) to improve the boundary conditions by considering adaptive schemes to apply radiative conditions as proposed by Marchesiello et al. (2001); (3) to improve the vertical mixing scheme in order to obtain a better picture of entrainment (and possibly detrainment) in the Gulf of Cadiz; and (4) to consider variables in time conditions at the Strait of Gibraltar, which may be important for a better understanding of variability at Mediterranean Water levels. Finally, we should point out that some investigation was done using mixed vertical coordinates (e.g. sigma close to the bottom and Cartesian above). Results were promising, but there is room for future improvement as some problems persist at the open boundaries.

Acknowledgements

The OMEX II–II project is financed by the European Union MAST III programme under contract number MAS3-CT97-0076.

References

Abbot, M.B., Damsgaardand, A., Rodenhuis, G.S., 1973. System 21, Jupiter, a design system for two-dimensional nearly-horizontal flows. J. Hydrol. Res. 1, 1–28.

Ambar, I., Fiúza, A., Boyd, T., Frouin, R., 1986. Observations of a warm oceanic current flowing northward along the coasts of Portugal and Spain during Nov–Dec 1983. Eos Trans. AGU 67 (144), 1054.

Arakawa, A., Lamb, V., 1977. Computational design of the basic dynamical processes of the UCLA general circulation model. Methods Comput. Phys. 17, 174–267.

Arhan, M., Billant, A., Colin de Verdiére, A., Daniault, N., Prego, R., 1991. Hydrography and velocity measurements offshore from the Iberian Peninsula. Bord-Est Data Report, vol. 2. Campagnes Oceanographiques Françaises, No 15. IFREMER Publications, Brest, France.

Arhan, M., Colin de Verdiére, A., Mémery, L., 1994. The Eastern Boundary of the Subtropical Atlantic. J. Phys. Oceanogr. 24, 1295–1316.

Bakun, A., Nelson, C.S., 1991. The seasonal cycle of wind-stress curl in subtropical Eastern Boundary Current regions. J. Phys. Oceanogr. 21, 1815–1834.

Barnard, S., Barnier, B., Beckman, A., Boening, C., Coulibaty, M., DeCuevas, D., Dengg, J., Dieterich, C., Ernst, U., Herrmann, P., Jia, Y., Killworth, P., Kroeger, J., Lee, M., Le Provost, C., Molines, J.-M., New, A., Oschlies, A., Reynauld, T., West, L., Willebrand, J., 1997 September. DYNAMO: Dynamics of North Atlantic Models: Simulation and assimilation with high-resolution models. Berichte aus dem Institut fuer Meereskunde an der Christian-Albrechts-Universitat Kiel, no. 294, 334 pp. ISSN 0341-8561.

Batteen, M.L., Rutherford, M.J., 1990. Modeling studies of eddies in the Leeuwin Current: the role of thermal forcing. J. Phys. Oceanogr. 20, 1484–1520.

Batteen, M.L., Haney, R.L., Tielking, T.A., Renaud, P.G., 1989. A numerical study of wind forcing of eddies and jets in the California Current System. J. Mar. Res. 47, 493–523.

Batteen, M.L., Rutherford, M.J., Bayler, E.J., 1992. A numerical study of wind- and thermal-forcing effects on the ocean circulation off western Australia. J. Phys. Oceanogr. 22, 1406–1433.

Batteen, M.L., Martinez, J.R., Bryan, D.W., Buch, E.J., 2000. A modeling study of the coastal eastern boundary current system off Iberia and Morocco. J. Geophys. Res. 105, 14173–14195.

Burchard, H., Bolding, K., Villarreal, M.R., 1999. GOTM, A Gen-

eral Ocean Turbulence Model. Theory, implementation and test cases. Rep. of EC, EUR 18745 EN.

Cancino, L., Neves, R.J., 1998. Hydrodynamic and sediment suspension modelling in estuarine systems. Part II: Application in the Scheldt and Gironde Estuaries. J. Mar. Syst. 22, 117–131.

Coelho, H.S., Neves, R.J.J., Leitão, P.C., Martins, H., Santos, A., 1999. The slope current along the Western European Margin: a numerical investigation. Oceanography of the Iberian Continental Margin. Bol. Inst. Esp. Oceanogr. 15, 61–72.

Daniault, N., Mazé, J.P., Ahran, M., 1994. Circulation and mixing of Mediterranean Water west of the Iberian Peninsula. Deep-Sea Res. 41, 1685–1714.

Fiúza, A.F.G., Dias, J.H., Alonso, J., 1996. Long-term current measurements on the West Iberian margin. MORENA Scientific and Technical Report No 36. Instituto de Oceanografia, University of Lisbon, Lisbon, Portugal.

Fiúza, A.F.G., Hamann, M., Ambar, I., Diaz del Rio, G., Gonzáles, N., Cabanas, J.M., 1998. Water masses and their circulation off western Iberia during May 1993. Deep-Sea Res. 45, 1127–1160.

Flather, R.A., 1976. A tidal model of the nothwest European continental shelf. Mem. Soc. R. Sci. Liege, Ser. 6 (10), 141–164.

Frouin, R., Fiúza, A., Ambar, I., Boyd, T.J., 1990. Observations of a poleward surface current off the coasts of Portugal and Spain during the winter. J. Geophys. Res. 95, 679–691.

Gaspar, P.G., Grégoris, Y., Lefevre, J.-M., 1990. A simple eddy kinetic energy model for simulations of the oceanic vertical mixing: tests at station Papa and Long-Term Upper Ocean Study site. J. Geophys. Res. 95, 16179–16193.

Haney, R.L., 1985. Midlatitude sea surface temperature anomalies: a numerical hindcast. J. Phys. Oceanogr. 8, 363–392.

Haynes, R., Barton, E.D., 1990. A poleward flow along the Atlantic coast of the Iberian peninsula. J. Geophys. Res. 95, 11141–11425.

Haynes, R., Barton, E.D., Pilling, I., 1993. Development, persistence and variability of upwelling filaments off the Atlantic coast of the Iberian Peninsula. J. Geophys. Res. 98, 22681–22692.

Huthnance, J.M., 1984. Slope currents and ''JEBAR''. J. Phys. Oceanogr. 14, 795–810.

Huthnance, J.M., van Aken, H., White, M., Barton, E.D., LeCann, B., Coelho, E.F., Fanjul, E.A., Miller, P., Vitorino, J., 2002. Ocean margin exchange — water flux estimates. J. Mar. Syst. 32, this issue.

Jungclaus, J.H., Mellor, G.L., 2000. A three-dimensional model study of the Mediterranean outflow. J. Mar. Syst. 24, 41–66.

Klein, B., Siedler, G., 1989. On the origin of Azores Current. J. Geophys. Res. 94, 6159–6188.

Leendertse, J., 1967. Aspects of a computational model for long water wave propagation, Memorandum RH-5299-RR, Rand, Santa Monica.

Leendertsee, J., Liu, S., 1978. A three-dimensional turbulent energy model for non-homogeneous estuaries and coastal sea systems. In: Nihoul, J. (Ed.), Hydrodynamics of Estuaries and Fjords. Elsevier, Amsterdam, pp. 387–405.

Levitus, S., Boyer, T.P., 1994. World Ocean Atlas 1994. Vol. 4: NOAA Atlas NESDIS 4, 117 pp.

Levitus, S., Burgett, R., Boyer, T.P., 1994. World Ocean Atlas 1994. Vols. 1 and 2: NOAA Atlas NESDIS 3, 99 pp.

Lopes da Costa, C.N., 1991. Simulações da corrente forçada pelo vento na costa de Portugal. PUB (G)-IH-210-DT, Instituto Hidrográfico da Marinha, Lisbon, Portugal, 110 pp.

Marchesiello, P., McWilliams, J.C., Shchepetkin, A., 2001. Open boundary conditions for long-term integration of regional oceanic models. Ocean Modell. 3, 1–20.

Martins, F.A., Neves, R.J., Leitão, P.C., 1998. A three-dimensional hydrodynamic model with generic vertical coordinate. In: Babovic, V., Larsen, L.C. (Eds.), Proceedings of Hidroinformatics98, Copenhagen, Denmark, August 1998, vol. 2. Balkema, Rotterdam, pp. 1403–1410.

Martins, H., Santos, A., Coelho, E.F., Neves, R., Rosa, T.L., 1999. Numerical simulation of internal tides. J. Mech. Eng. Sci. 214C, 867–872.

Martins, F.A., Leitão, P.C., Silva, A., Neves, R., 2001. 3D modelling of the Sado Estuary using a new generic vertical discretization approach. Oceanol. Acta. 24, S51–S62.

Mauritzen, C., Morel, Y., Paillet, J., 2001. On the influence of Mediterranean water on the central waters of the North Atlantic Ocean. Deep-Sea Res. 48, 347–381.

Mazé, J.P., Ahran, M., Mercier, H., 1997. Volume budget of the eastern boundary layer off the Iberian Peninsula. Deep-Sea Res. 44, 1543–1574.

McCreary, J.P., Shetye, S.R., Kundu, P., 1986. Thermohaline forcing of eastern boundary currents: with application to the circulation off the west coast of Australia. J. Mar. Res. 44, 71–92.

McCreary, J.P., Kundu, P., Chao, S.Y., 1987. On the dynamics of the California current system. J. Mar. Res. 45, 1–32.

Miranda, R., Neves, R., Coelho, H., Martins, H., Leitão, P.C., Santos, A., 1999. Transport and mixing simulation along the continental shelf edge using a Lagrangian approach. Bol. Inst. Esp. Oceanogr. 15, 39–60.

Oey, L., Chen, P., 1992. A model simulation of circulation in the Northeast Atlantic shelves and seas. J. Geophys. Res. 97, 20087–20115.

Paillet, J., Mercier, H., 1997. An inverse model of the eastern North Atlantic general circulation and thermocline ventilation. Deep-Sea Res. 44, 1293–1328.

Palma, E.D., Matano, R.P., 2000. On the implementation of passive open boundary conditions for a general circulation model: the three-dimensional case. J. Geophys. Res. 105, 8605–8627.

Relvas, P., 1999. Dynamics of the Cape São Vicente upwelling region observed from sea, land and space. PhD Thesis, School of Ocean Sciences, University of Wales, 244 pp.

Røed, L.P., Shi, X.B., 1999. A numerical study of the dynamics and energetics of cool filaments, jets and eddies off the Iberian Peninsula. J. Geophys. Res. 102, 29817–29841.

Santos, A.J.P., 1995. Modelo hidrodinâmico de circulação oceânica e estuarina (in Portuguese). PhD Thesis, IST Lisbon, 273 pp.

Saunders, P.M., 1982. Circulation in the eastern North Atlantic. J. Mar. Res. 40, 641–657.

Stevens, I., Hamann, M., Johnson, J., Fiúza, A., 2000. Comparisons between a fine resolution model and observations in the Iberian shelf-slope region. J. Mar. Syst. 26, 53–74.

Taboada, J.J., Prego, R., Ruiz-Villarreal, M., Montero, P., Gómez-Gesteira, M., Santos, A.P., Pérez-Villar, V., 1998. Evaluation of the seasonal variations in the residual patterns in the Ria de Vigo

(NW Spain) by means of a 3D baroclinic model. Estuarine, Coastal Shelf Sci. 47, 661–670.

Trenberth, K.E., Large, W.G., Olsen, J.G., 1990. The mean annual cycle in global wind stress. J. Phys. Oceanogr. 20, 1742–1760.

Vinokur, M., 1989. An analysis of finite-difference and finite-volume formulations of conservation laws. J. Comput. Phys. 81, 1–52.

Visbeck, M., Marshall, J., Haine, T., Spall, M., 1997. Representation of topography by shaved cells in a height coordinate ocean model. Mon. Weather Rev. 125, 2293–2315.

Weaver, A.J., Middleton, J.H., 1990. An analytic model for the Leeuwin Current off western Australia. Cont. Shelf Res. 10, 105–122.

White, M., 1998. Shelf slope observations. Ocean Margin Exchange OMEX II-PhaseII, First Annual Science Report, Université Libre de Bruxelles, Universitetet I Tromsø, Plymouth Marine Laboratory, Nederlands Institut voor Onderzoek der Zee, Proudman Oceanographic, 139–147.

Zenk, W., Armi, L., 1990. The complex pattern of Mediterranean Water off the Portuguese continental slope. Deep-Sea Res. 37, 1805–1823.